A STUDY OF THE TEMPERATURE DEPENDENCE OF TWO-GAMMA ANNIHILATION OF POSITRONS IN ZINC

A Thesis

Submitted to

the Faculty of Graduate Studies

University of Manitoba

In Partial Fulfillment

of the Requirements for the Degree

Master of Science

---

by

Maximilian Buchheit

Winnipeg, Canada

March 1973

TABLE OF CONTENTS

LIST OF FIGURES

ACKNOWLEDGEMENTS

I would like to thank my supervisor, Dr. B. G. Hogg, for his guidance and encouragement, and above all, his patience throughout the course of this work.

I would also like to thank my colleagues, Drs. A. G. Gould, E. Becker and E. Senicki for their helpful discussions and advice, Dr. R. West who originally suggested the experiment, and of course, my wife, for bravely taking on the task of typing this thesis.

ABSTRACT

The temperature dependence of the angular distribution of gamma rays from annihilating electron-positron pairs in poly-crystalline and single crystal samples of zinc has been studied with a modification of the conventional long-slit angular correlation apparatus.

Results show that there is a systematic difference in the temperature dependence of poly and single crystal samples of zinc. This difference is interpreted from an analysis of the results and hypotheses of previous workers, as arising most probably from the diffraction of positrons from the surface of the crystal. Other probable mechanisms are also discussed.

This work has determined a drop in integrated count rate of 2.41% ± 0.66% for the single crystalline sample of zinc and a drop of 0.72% ± 0.66% for the poly-crystalline sample, in going from 293°K to 185.5°K (well below the Debye temperature for zinc). No such changes within experimental error, have been observed above 300°K.

CHAPTER ONE

INTRODUCTION

1.0

Since the existence of the positron was first postulated by Dirac in 1930 and verified experimentally by Anderson in 1932, it has become the focus of intense study, and more recently, a valuable aid to research in organic chemistry and the physics of the solid state, notably the study of metals and alloys (Goldanskii, 1968; Proceedings of the Second International Positron Conference, Kingston, Canada, 1971).

Fundamentally, this interest stems from the nature of the interactions of positrons with matter and can be understood on the basis of quantum electrodynamics (Heitler, 1954). Indeed the experimental verification of the existence of a hydrogen-like bound state of the positron-electron system (Shearer and Deutsch, 1949), originally suggested by Mohorovicic in 1934 and subsequently named 'Positronium' by Ruark in 1945, did much to further the validity of quantum electrodynamic theory.

1.1 Annihilation Process

Let us consider the possible modes of annihilation of a free positron-electron pair, not in a bound state. Under such simplified conditions the pair may annihilate with the subsequent

creation of gamma-ray quanta so that energy and momentum are conserved. That only two and three quanta annihilations are statistically most probable becomes apparent from the symmetry and parity arguments set forth by Yang (C.N.Yang, 1950).

If the two particles are at rest relative to one another, then two or more quanta must be emitted to conserve linear momentum. As seen from Diagram 1, two quanta, each of $2m_o c^2$ energy, are produced at 180° to one another, only if the pair is in the 'singlet' state, whereas three quanta are produced only if the pair is in the 'triplet' state. Note that the distribution of the total energy (equal to $2m_o c^2$) between the three quanta is no longer uniquely determined by the relative directions of propagation. In general the selection rules developed by Yang permit an even number of quanta for the singlet state and an odd number for the triplet state, but cross sections for more than 3-quanta annihilations are exceedingly smaller than for the processes discussed above (Goldanskii, 1968).

We shall not dismiss single quantum and zero quantum annihilation processes as these are possible if a many body interaction or collective excitation exists whereby energy and momentum are conserved. A likely candidate for such a process is given by the Feynman diagram 2(c) (after Goldanskii, 1968) where an external nucleus or electron is present to absorb recoil momentum. Conceivably, two such external agents may result in no gamma rays being produced; in a lattice, a phonon interaction may be possible. However, cross-sections for such processes are

Figure 1

Modes of Annihilation

ANTI-PARALLEL SPIN STATE
('SINGLET' , $\sigma = 0$)

PARALLEL SPIN STATE
('TRIPLET' , $\sigma = 1$)

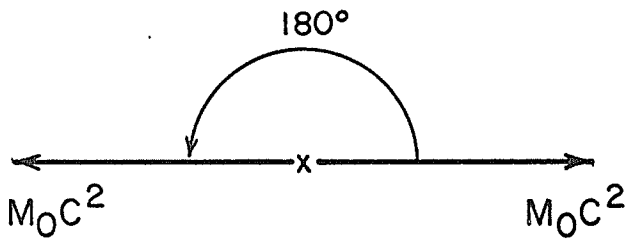

$2-\gamma$ (Collinear)

FIG. 1 (a)

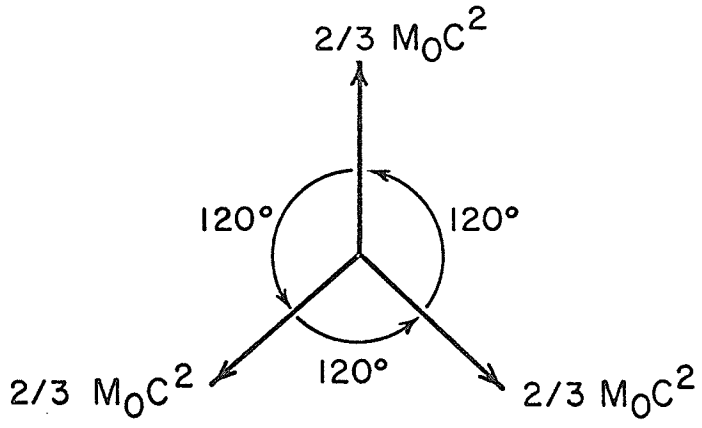

$3-\gamma$ (Co-planar)

FIG. 1 (b)

Figure 2

Feynman Diagrams of Annihilation Modes

Figure 3

Scattering Relationships in the C.M. and Lab Frames

Fig. 2

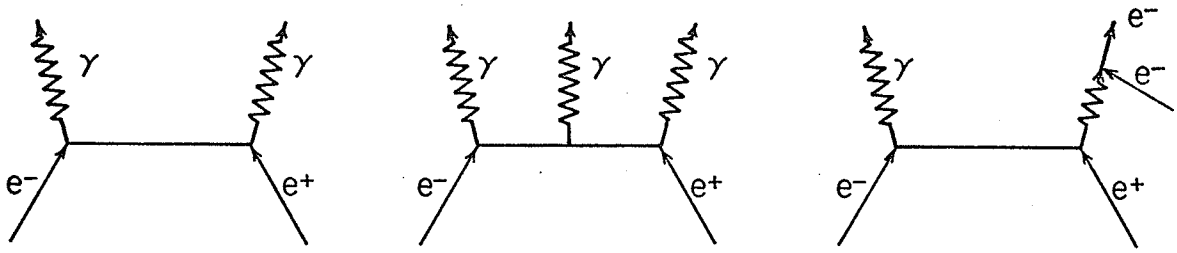
γ
γ
e⁻
e⁺
2−γ
γ
γ
γ
e⁻
e⁺
3−γ
γ
e⁻
e⁻
e⁻
e⁺
Possible method
of single−γ

Fig. 3

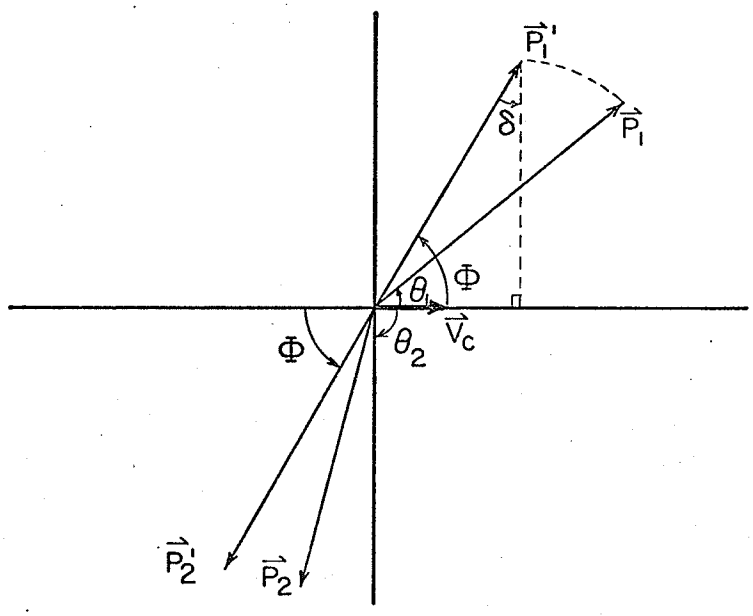
$\vec{P}_1'$
$\vec{P}_1$
δ
Φ
θ₁
θ₂
Φ
$\vec{V}_c$
$\vec{P}_2'$
$\vec{P}_2$
$V_c \ll C$

smaller than that for the two-gamma annihilation by an order of α^4 (where α is the fine structure constant equal to 1/137). In turn, the two-gamma to three-gamma cross section ratio has been calculated to be:

$$(1) \qquad \sigma_{2\gamma}/\sigma_{3\gamma} = 1115$$

for the case of a free unbound pair (Ore and Powell, 1949).

If positronium has been formed, we must account for the relative abundance of the singlet (para) and triplet (ortho) states; that is, since the triplet (1^3S) state may have m equal to -1,0,+1 whereas (1^1S) only has m equal to 0, resulting in a 3:1 ratio of abundance. Thus for the bound Ps state:

$$(2) \qquad \sigma_{2\gamma}/\sigma_{3\gamma} = 1115/3 = 372$$

1.2 Type of Experiments Done

It is for this reason, and also since triple- coincidence experiments yield less useful information, that most experimental efforts concentrate on two-gamma annihilation. These take the form of two-gamma annihilation lifetime measurements and two-gamma angular correlation. Lifetime measurements are of value in the study of positronium chemistry in various organic systems and in insulators (Goldanskii, 1968), as the time resolution

limits of the latest commercially available equipment is more than sufficient. However, lifetime studies in metals have been hindered in the past by the inability to resolve the very fast components present (of sub-nano second order) so that usage has been somewhat restricted (R. N. West, 1971).

Angular correlation is by far the more widely used tool, since it is both simpler, and resolution limits are more dependent upon the apparatus geometry, and of source-sample arrangement. Furthermore it has achieved modest success in the study of metals (Stewart and Roellig, 1967; Kingston Positron Conference Proc., 1971) providing a proving ground for current electronic Hartree-Fock band calculations (Gould, 1972). This current work stems from a need to resolve apparent temperature anomalies found in the wealth of previous angular correlation experiments in metals (see section 1.5).

1.3 Angular Correlation of Two-gamma Annihilation Radiation

Let us suppose that positrons within a sample have thermalized sufficiently so that if we consider the velocity of an electron-positron pair $\vec{V}_c$ prior to annihilation it will be non-relativistic. Conservation of momentum and energy still hold for the annihilation event, taking into account the rest energy of the pair.

We may solve this two-body (exergodic) scattering problem in the centre-of-mass frame and then transform back to the

laboratory frame (keeping in mind, that we must undergo a Lorentz transformation to do so, since the gamma-rays travel at the speed of light). There is, of course, one remaining degree of freedom in the solution (see Appendix I for a detailed analysis), which we choose to be the scattering angle Φ . We see then, that in the C.M. frame, the gamma-rays are emitted anti-parallel to one another, and share identical energies equal to :

$$(3) \qquad E_{\gamma}^{C.M.} = mc^2 \ (1+ 1/2 \cdot V_c^2/c^2 \ )$$

However, in the lab frame, we detect not only a deviation from 180° for the angle of separation, but also a Doppler-shifted difference in the observed energies, both proportional to the ratio (V_c /C). Referring to diagram 3, we see the possible relationships between the scattered photons (Φ is the scattering angle in the C.M. frame of gamma-ray 1 with respect to the incident direction of the C.M., whereas θ_1 is the corresponding angle in the lab frame). Then we see that:

$$(4) \qquad \cot \theta_1 \doteq \frac{((\cos \Phi + 2(V_c/c) \ )}{\sin \Phi} + \mathcal{O}(V_c^2/c^2)$$

We note that for $\Phi = 90^\circ$, $\cot \theta_1 \doteq 2V_c/c$ whereas if $V_c = 0$, then the two gamma-rays would remain 180° apart in the lab frame. In practice however, we measure the complement of θ, 2α, so that the deviation from 180° is given by:

$$(5) \qquad 2\alpha \simeq \tan 2\alpha = 2(V_c/c) + \mathcal{O}(V_c^2/c^2)$$

and the momentum of the electron is given by:

$$(6) \qquad p = mc\alpha$$

These results are exact to within an order of (V_c^2/c^2), as the present angular resolution of the typical apparatus is only of the order of 1/2 milliradian, too large to warrant further relativistic corrections.

The measured energies in the lab frame, are no longer neccessarily equal but differ by an amount:

$$(7) \qquad \Delta E_\gamma \simeq E_T(V_c/c) \cos \Phi + \mathcal{O}(V_c^2/c^2)$$

so that for $\Phi=90^\circ$ the energies are unchanged, but for $\Phi=0^\circ$ or 180° they differ by $E_T(V_c/c)$ where E_T is the total energy of the system (Appendix I).

Original arrangements to measure the angular correlation of two photon annihilation were developed by Beringer and Montgomery in 1942. Subsequent workers have since then highly refined the apparatus and the analysis of the data (De Benedetti et al, 1950) to do extensive work on gases (see review by Goldanskii, 1968), organic liquids (Kerr and Hogg, 1962; Chuang and Hogg, 1967), and on metals (Stewart et al, 1962; Berko and Plaskett, 1958). More recently, the study of metals and alloys

with a point-slit geometry (as opposed to the conventional long-slit) apparatus has proved to be particularly fruitful (Becker et al, 1969; Senicki et al, 1972). A further description of a long-slit apparatus is given Chapter 2.

1.3.1 Analysis of Long Slit Angular Correlation Results

Analysis of long-slit results has in the past followed that of De Benedetti (1950) and Stewart (1957). The experimental long-slit count rate may be written as:

$$N(P_z) = A \int_{-\infty}^{\infty}\int_{-\infty}^{\infty} \rho(\vec{p})\ dp_x dp_y \qquad (8)$$

where A is a normalization constant and $\rho(\vec{p})$ is the probability density of the annihilating pair having a momentum $\vec{p}$.

If one assumes that $\rho(\vec{p})$ is isotropic, then we may eliminate the angular dependence and write instead:

$$N(p_z) = 2\pi A \int_{P_z}^{\infty} p\ \rho(p)\ dp \qquad (9)$$

from which we obtain (using $p_z = mc\alpha$):

$$\rho(p_z) = -[2\pi A(mc)^2]^{-1}\alpha^{-1}\frac{dN}{d\alpha}(\alpha) \qquad (10)$$

This result is in simple form, and facilitates analysis of the raw data by computer.

However, this analysis is only valid and useful for substances having an isotropic structure or high symmetry, which is the case for most organic compounds (liquid and gaseous) that have been studied in the past, and clearly can not achieve much success in the study of metals where it is necessary to construct a positron wave function which retains proper crystal symmetry (Stroud and Ehrenreich, 1968; A. G. Gould et al, 1972).

Furthermore, we have assumed that no resolution limitations exist. To be more exact, we must express the experimental count rate as a convolution of the true count rate with the resolution function $r(\vec{p})$ of the apparatus (usually determined analytically or by computer simulation) so that:

$$C(p_z) = \int \rho(\vec{p}') \; r(\vec{p}'-\vec{p}\,) \; d^3p' \qquad (11)$$

No agreement as to how to deconvolute such an integral has been reached (Since only finite data are available and the limits of integration extend to only 20 to 30 milliradians at the most, considerable information is either lost or not present, making some methods impractical and untrustworthy). Most commonly used is an iterative scheme whereby a trial distribution ρ' is folded with the resolution function, compared with the observed count rate $C(p_z)$ and then re-adjusted, point by point, until some convergence criterion is reached (W.H. Holt, PhD thesis, 1967; P.C. Lichtenburger et al, Proc. of Kingston Positron Conference, 1971).

The starting point for all theoretical calculations which ultimately attempt to simulate or 'fit' the data is the independent particle approximation for the interaction of a positron-electron pair (Ferrell, 1956). Treating the problem as one of scattering from an initial state where the pair is present with momentum $\vec{p}$, to a final state where it is absent with the propagation of two gamma-rays having net momentum $\vec{p}$, then the matrix element for the transition is proportional to:

$$\int_V \exp(i\vec{p}\cdot\vec{r}/\hbar)\,\psi_+(\vec{r})\,\psi_n(\vec{r})\,d^3r \tag{12}$$

where ψ_+ and ψ_n are the wavefunctions for the positron and the n'th electron respectively. Then the probability of the pair having momentum within d^3p of $\vec{p}$ is given by:

$$\rho_n(\vec{p}) \propto \left| \int_V e^{i\vec{p}\cdot\vec{r}/\hbar}\,\psi_+(\vec{r})\,\psi_n(\vec{r})\,d^3r \right|^2 \tag{13}$$

We may obtain the average lifetime of the positron in the substance by summing over all possible momenta and electrons. Thus:

$$\tau^{-1} \propto \sum_n \int d^3p\,\rho_n(\vec{p}) \tag{14}$$

The specific problem at hand is the proper evaluation of ψ_+ for the system being studied, if information upon the electronic states is available. Gould (Ph.D. thesis, 1972) has done

extensive calculations for metals of cubic and hexagonal structure, obtaining positron wavefunctions with the proper crystal symmetry. Chuang (Ph.D. thesis, 1968) has done work on complex organic molecules.

1.4 Thermalization of the Positron

In all the previous discussion it has been assumed that the positron has been effectively thermalized (i.e. its kinetic energy amounts to no more than kT - about 1/40 eV at room temperature) before annihilation takes place. That this assumption is valid, is of primary concern in any of the work done in this field. If it were wrong it would not only affect lifetime spectra by limiting the possible resolution, but also complicate and obscure the analysis of angular correlation data if the positron were to retain even a few eV of energy (since in metals this would be of the same order as the Fermi energy) before annihilation.

Several workers have sought to calculate thermalization times in an electron gas (Garwin, 1953 and Lee-Whiting, 1955) and have found values of 10^{-12} to 10^{-13} seconds, well below the measured lifetimes in metals ($\simeq 10^{-10}$ sec) so that the basic assumption was accepted as valid. More recent work by Carbotte and Arrora (1967) (modifying Lee-Whiting's calculations by use of the Thomas-Fermi screening parameter) verifies that at high temperatures ($\geqslant 300^{\circ}K$) the thermalization time is much less than

the annihilation lifetime. Simply stated, an incoming energetic positron may scatter electrons only into unoccupied states (because of the Pauli exclusion principle) which lie within kT or above the Fermi energy. Thus, an incoming positron will on the average be scattered to a lower energy and will eventually become thermalized after several scattering events. However, at low temperatures the positron may annihilate before complete thermalization has taken place (eg. at annihilation in Na, the positron has an energy of $\simeq$ .013 eV at low temperatures; this is higher than kT but perturbs the angular correlation by an amount too small to be seen within the limits of the apparatus). This effect of non-thermalization decreases with increasing temperature until a temperature is reached above which the thermalization time becomes increasingly shorter than the annihilation lifetime.

1.5 The Temperature Anomaly Problem in Metals

From the discussion in the above section, it is apparent that retention of some of the positron's initial energy could affect the nature of both the angular correlation and lifetime spectra experiments (see Chapter 4). In the past decade various workers have observed changes in the angular correlation curves of metals which are dependent upon temperature, and which have stimulated frequent exchanges of differing explanations. Dekhtyar first reported (1961) changes in the total normalization (taken

as the area of the count rate curve) and of the shape of angular correlation curves for bismuth and zinc, observing that both the area of the curve and its F.W.H.M. decreased with temperature. His tentative hypothesis was that a single-gamma process or a phonon-positron interaction played a role in depleting the total number of positrons annihilating by the two-gamma process, was discounted by the work done by Faraci et al (1969).

Also working with a bismuth single crystal, they confirmed Dekhtyar's results, but used a poly-crystal of identical geometry as a control and found no effect present within experimental error. For the single crystal, the normalization decrease was 21% going from 300° K to 77° K and 28% going from 300° K to 4.2° K. However, no change in F.W.H.M. of the curves was observed. As we shall see in Chapter 4, interpretation of these results proved confusing. To further investigate the matter, the changes in area were measured for the region 0 to 20 milliradians which included more of the tails of the distribution and were found to be much less pronounced than those for the peak portion of the curve. The hypothesis put foward was that as the temperature decreased, the lower momentum components were depleted with accompanying broadening of the tails or higher momentum components. In a crude attempt to justify a process of interaction with an additional single phonon or conduction electron, they concluded that only a collective excitation could play a role since the momentum required was too large for a single particle and also the effect was only present in an ordered lattice (single crystal).

Dekhtyar (1969), while in general agreement with these results, proposed that the mechanism responsible for the temperature effect in single crystals (but not in poly-crystals), was the channeling of positrons with their subsequent ejection from the crystal. However, in testing the hypothesis, the data from the initial experiment of eight years before (Dekhtyar, 1961) was used in his analysis. Faraci et al (1970a) showed experimentally that ejection of positrons from the crystal was not possible (see Chapter 4 for further discussion) but that channeling, itself as a mechanism was not to be discounted. This they supported in a later experiment (1970b) done on several metals of different atomic number and found that in addition to no effect being found in poly-crystalline samples of each of these metals, the temperature effect in the single crystal samples was proportional to $Z^{3/2}$ in agreement with the theory of channeling of positrons (which is similar to that of protons - E. Uggerhoj, 1966).

Dekhtyar altered his basic hypothesis (Dekhtyar, 1969) by considering the diffraction of positrons either off the face of the crystal, or its interior with subsequent channeling out of the face, and presented experimental evidence to support this contention. However, not only was this in direct contradiction to the negative results of lifetime spectra done by Faraci et al (1970a) previously mentioned, but also the results of his experiment tended to support Faraci's channeling contention (1970b) at the sake of contradicting his own hypothesis.

It is interesting to note that Hyodo et al (1971) have shown that diffraction of the annihilation of gamma-rays by heavy metals occurs resulting in a measurable anistropy of the angular correlation curve, and further support their evidence by semi-empirical theory. Resultant changes were of the order of a 3% decrease in the peak of the curve and an increase at higher momenta. Since this process is temperature-susceptible, the possibility that it plays some role in the effect should not be dismissed.

Despite the complexity and diversity of results and hypotheses put forward, the present experiment was designed to shed further light upon the matter and to try to avoid the pitfalls of earlier attempts. The basic feature of the apparatus is the ability to measure almost the total area of the angular correlation curve, taking into account angles as far out as 34 milliradians, at various temperatures from above 300° K to 77° K without the need for point by point measurement of the angular distribution for each temperature. This enabled the typical run to be much faster with higher count rates and less electronic drift per run. With a conventional geometry, each run alone would take several weeks to complete, making temperature control over such a long period difficult. Efforts were concentrated on the changes in single and poly-crystalline samples of zinc. It is kept in mind, however, that due to serious malfunctions in the electronics, and various other minor but irritating technical problems, the completion of the experiment was delayed by one

year further. The apparatus is discussed in detail in the following chapter, and analysis and discussion of results appear in Chapters 3 and 4, where comparisons are made with results of previous authors.

CHAPTER TWO

EXPERIMENTAL APPARATUS

2.1 The General Apparatus Configuration

The angular correlation apparatus used employed a 'wide-slit' geometry which was easily adapted from a conventional double slit apparatus (see figures 1(a) and (b)) such as has been used quite often in the past (G. DeBlonde, PhD Thesis 1972). The apparatus sits rigidly upon a pair of 3" by 6" parallel aluminum I-beams to maintain alignment. The cryostat, housing the sample and source, sat between the two detectors at unequal distances from each. Both detectors were kept rigid and no movement was necessary. The detector collimating slits were made of 3" thick lead blocks, sufficently thick enough to cut the incident count of gamma rays of .511 MeV and 1.27 MeV energies to less than 0.2% of the direct beam through the slits. Main departures from the conventional apparatus arise in

a) the width of each slit,

b) the distance from the sample to each slit,

c) the restriction that the detectors are not moved but kept fixed and aligned at a zero angle of separation.

The 'narrow slit' detector collimator was 0.15 cm wide and was at a distance of 265 cm from the geometrical centre of the sample housing. The 'wide slit', on the other hand, was 140.3 cm from the sample housing, and was 7.14 cm square. This shape of

Figure 1

The Conventional and Wide-slit Apparatus Geometries

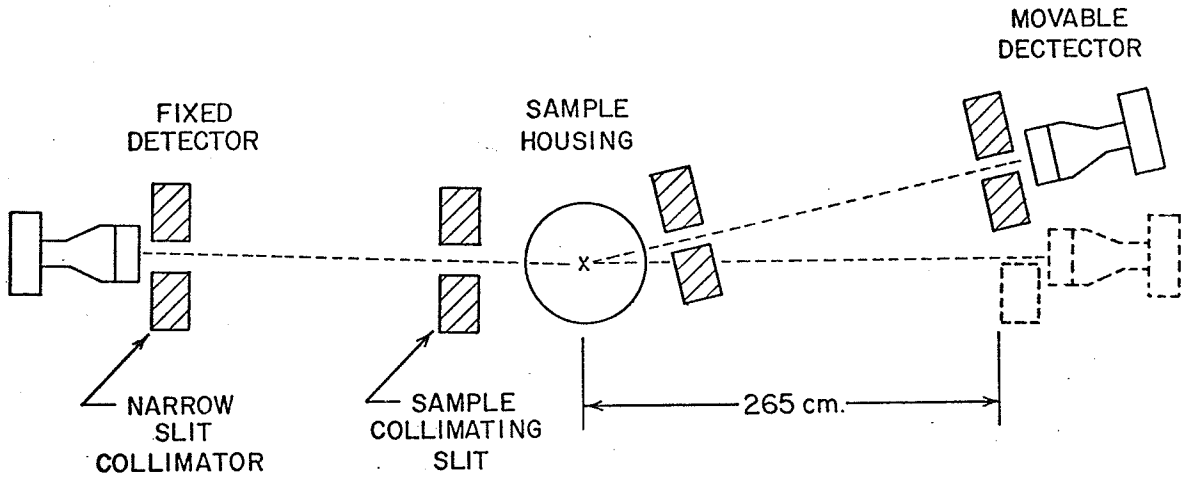

FIG. 1(a) CONVENTIONAL APPARATUS
(Not to scale)

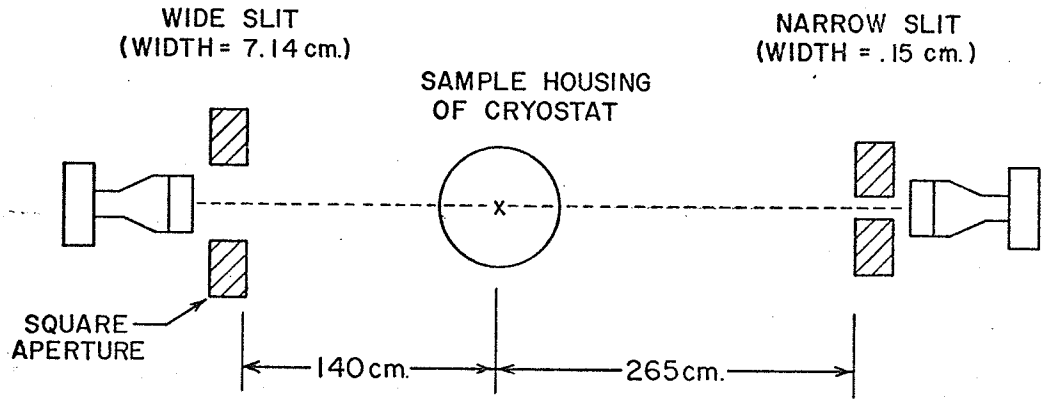

FIG. 1(b) WIDE SLIT APPARATUS
(Not to scale)

aperture was chosen to simplify analysis of the response function of the apparatus. No further collimation of the sample itself was necessary as the response (resolution) of the apparatus was insensitive to such measures. In effect, this arrangement of the apparatus achieved an integration of the angular dependent count rate over a total range of approximately 50 mrad (see Chapter 3 for a further discussion).

2.2 Supporting Electronics

Figure 2 illustrates briefly the arrangement of electronics used to observe and measure coincident count rates at various temperatures. The detectors consisted of Integral Assembly 16 MB4/A-X NaI(Tl) crystals which were 1" thick and 4" in diameter, mounted on 5018 HB photo-multiplier tubes. The detectors were driven by a Hamner N401 high voltage supply at a positive potential of one kilovolt. The negative signal pulse from the detector was inverted by a cathode follower amplifier with an output of approximately 1 volt which was sufficiently high enough to trigger the single channel analyzer. (Ortec model 486-amplifier, P.H.A.). Output pulses from both SCA's were fed into a slow coincidence unit (Ortec model 405, linear gate and slow coincidence). A Technical Measurement Corporation model SG-3A scaler was used to count the coincidence pulses on a free-run basis; that is, accumulation of counts was externally controlled by the Simplex model ET-100 timer-printer. The energy

Figure 2

Electronics Block Schematic

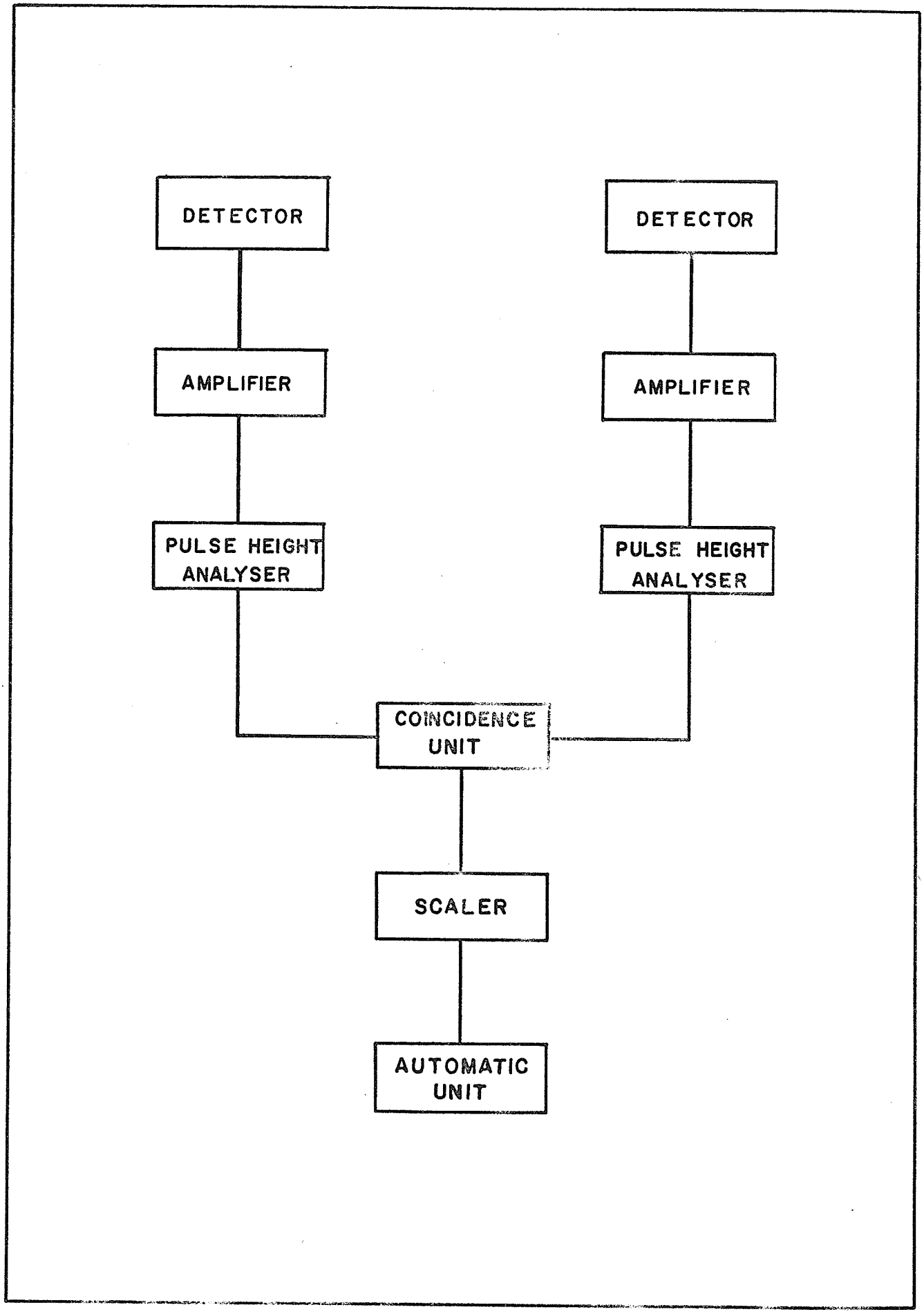
DETECTOR
DETECTOR
AMPLIFIER
AMPLIFIER
PULSE HEIGHT ANALYSER
PULSE HEIGHT ANALYSER
COINCIDENCE UNIT
SCALER
AUTOMATIC UNIT

windows on the single channel analysers were set to accept pulses corresponding to energies between 0.102 MeV and 0.715 MeV; this was sufficiently wide enough to accept Doppler-shifted 0.511 MeV annihilation radiation and yet still reject the accompanying 1.28 MeV gammas and low energy noise resulting from Compton scattered radiation.

Detector pulses were transmitted via 50 ohm/ft impedance cable with a properly matched impedance termination. Cable lengths were such that the resolution time of the coincidence unit stayed below 200 nanoseconds. The resolution time τ was determined experimentally by placing a source at each detector while keeping each isolated from the other by a large enough lead wall along the axis of the apparatus, thus assuring that the signals obtained by each detector were truly independent. One would then use the relationship

$$(1) \qquad N_{cc} = 2\tau N_1 N_2 \qquad \text{(Green and Lee, page 10)}$$

where N_1 , N_2 are the count rates of single events caught by the respective detectors, and N_{cc} is the chance count rate of pulses from both detectors which were resolved as being in coincidence by the electronics. These are totally chance coincidences since they originate from independent sources.

Using this method, τ was found to be approximately 160 nsec and remained unchanged after each run, the 'singles' count rate from each detector was recorded in order to arrive at an

estimate of the chance coincidence count background encountered during the run.

2.3 The Cryostat and Sample-Source Housing

2.3.1 The Upper Housing and Sample Holder

The cryostat, which also serves as the housing for source and sample, is basically of a simple design. Figure 3 illustrates the basic features of the structure, excluding some of the more intricate details which are explained below. The structure is mainly of brass, with all joints silver-soldered. The inner cylinder is a top-filling reservoir for liquid nitrogen and is suspended from the top by a vacuum tight solder joint. The bottom of the reservoir consists of a large thickness of copper, into which the sample holder may be screwed, forming a conventional 'cold finger' thermal contact. However, between the sample holder itself and the copper bottom of the reservoir, is a 'heat shunt' of mild steel, which lends a high heat capacity to the system. Although the system took longer to reach equilibrium with the heat shunt in place, it enabled gross temperature variations to be smoothed out over a longer time and provided a means of sustaining a low temperature even if the liquid nitrogen were suddenly depleted.

When the upper housing of the cryostat is sealed to a base via an O-ring seal, the interior can be evacuated by a roughing

Figure 3

Sample Housing and Cryostat

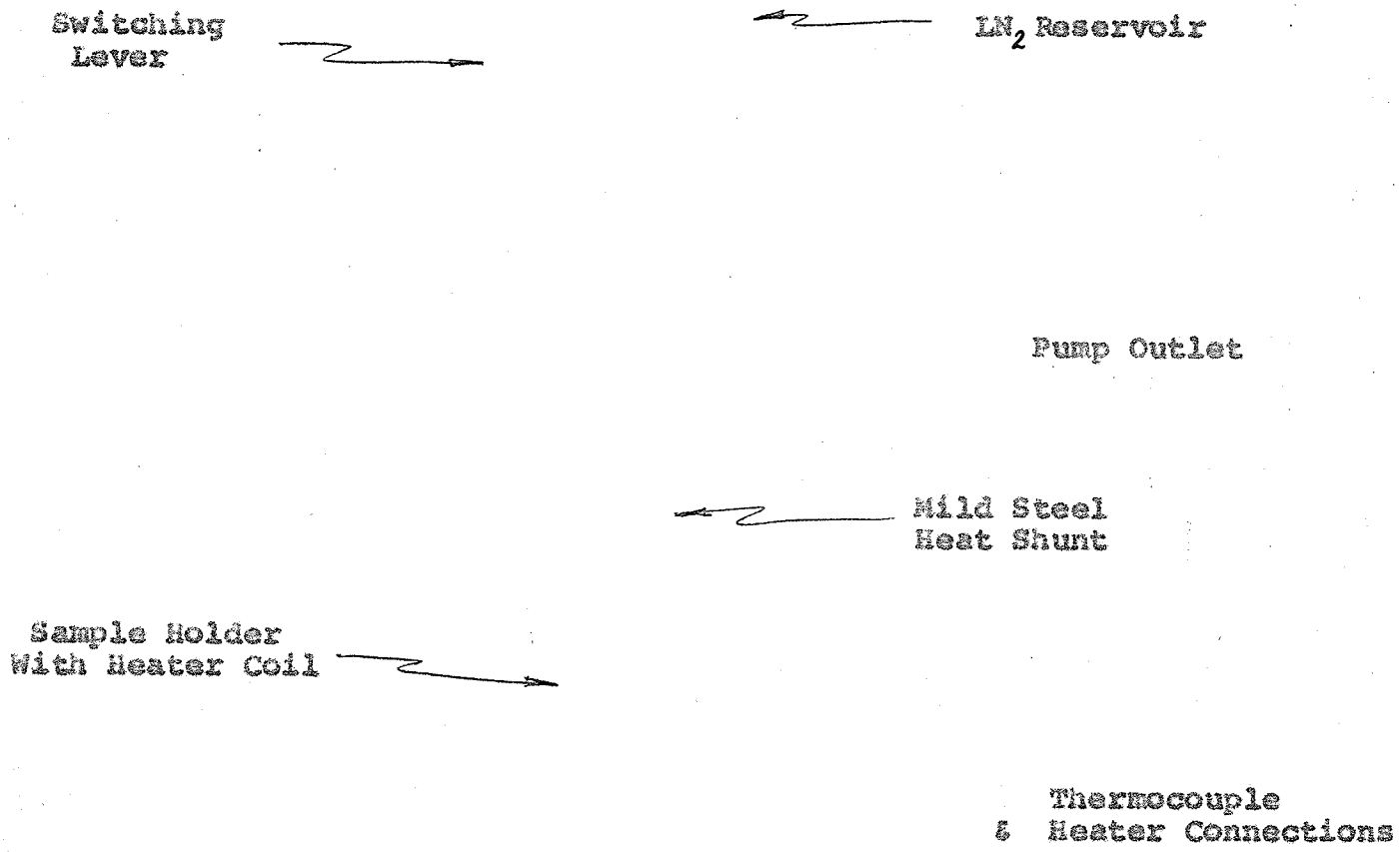

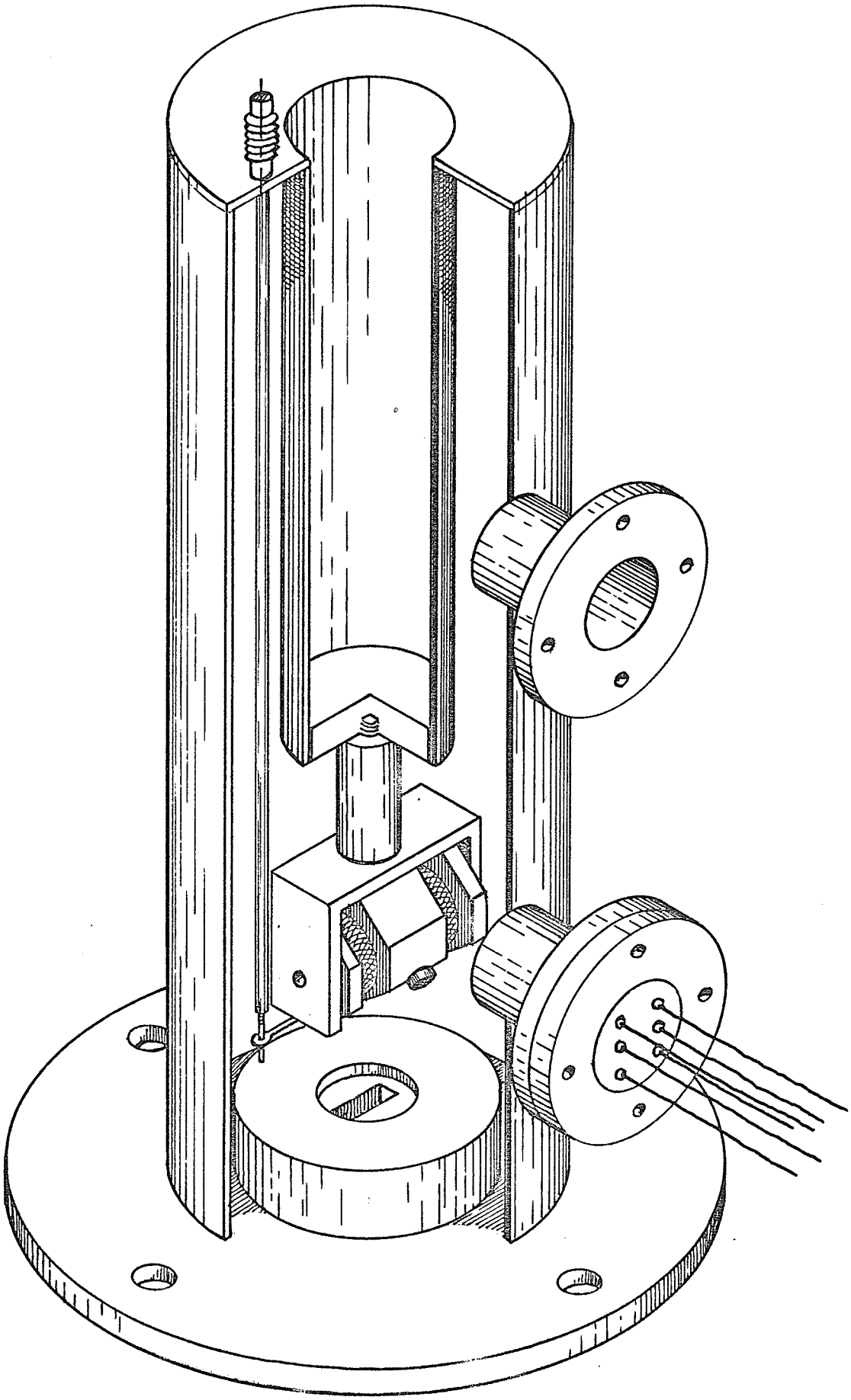

Figure 4

Sample Holder

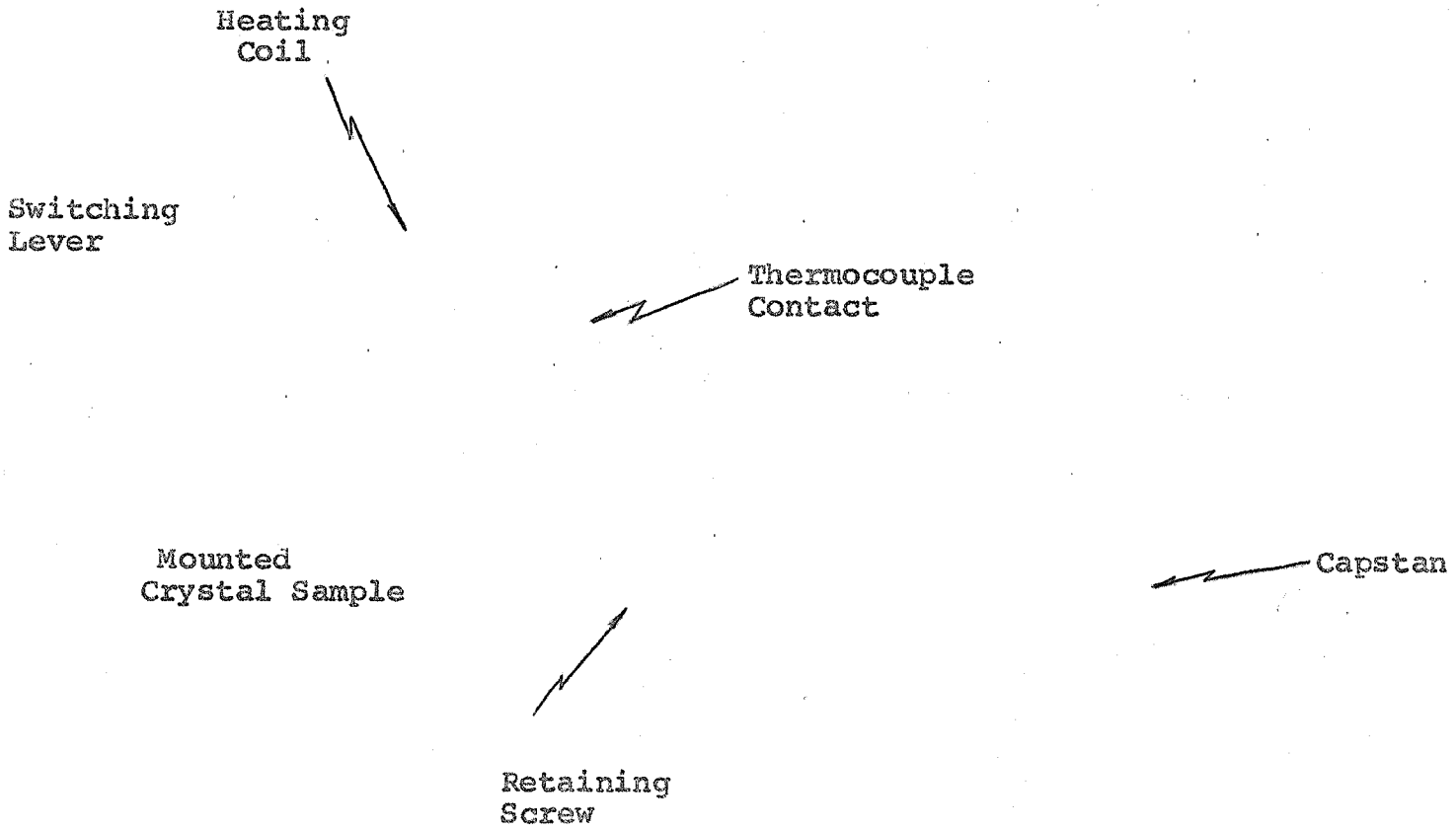

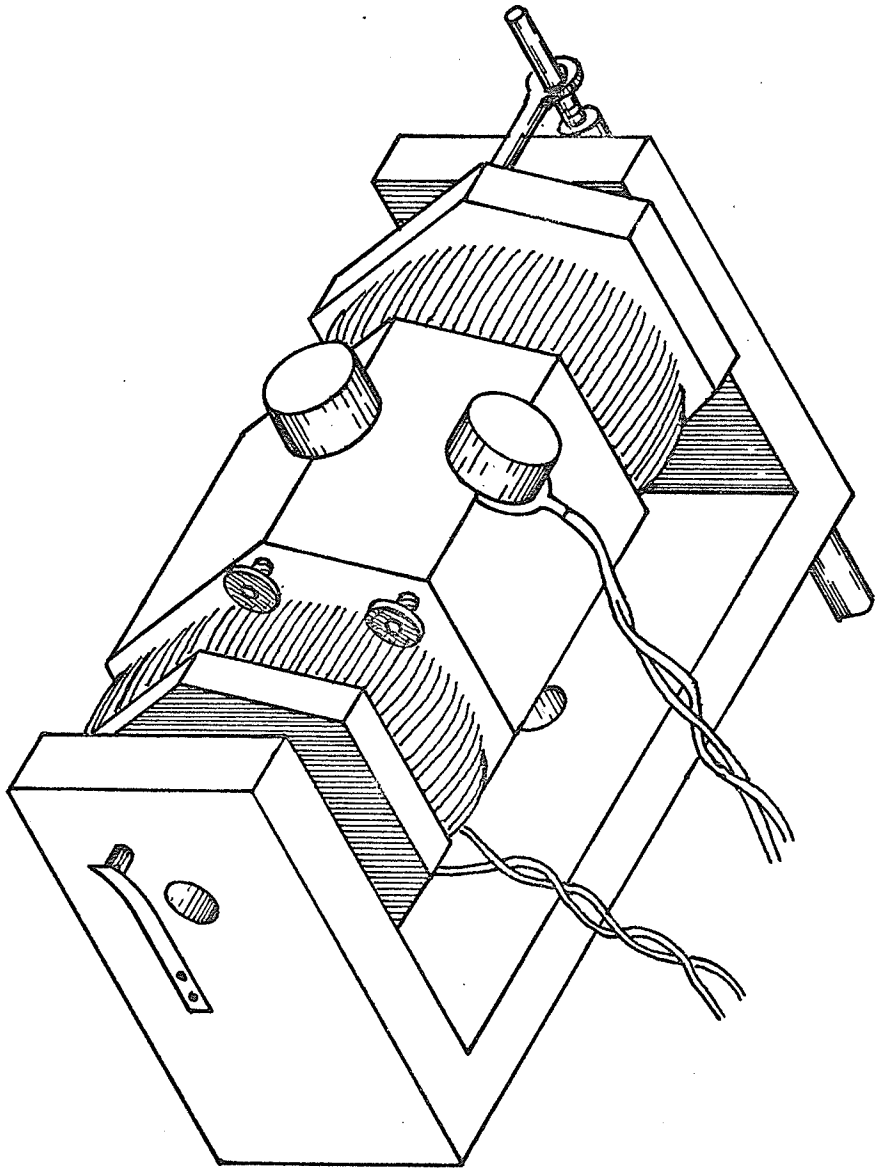

pump through the pump connection at the side. The typical vacuum achieved at room temperature was below 20 microns, sufficient for the purposes of the experiment.

Figure 4 illustrates the sample holder itself, designed to hold both the single crystal and polycrystalline samples at the same time. The holder was machined from a hexagonal brass piece to accomodate a heating coil of gauge 28 nichrome wire. The heating coil was built upon a initial layer of asbestos and electrically insulating ceramic cement which was also used to bond and insulate each successive layer of wire in the coil.

The crystal samples which were approximately 13.6 mm in diameter and 13.0 mm high were mounted on seats machined into the hexagonal holder so as to provide good thermal contact and just enough tolerance to allow later removal of the samples. Fine set screws were then used as retainer clamps for the samples. This mechanical means of mounting was deemed necessary, since it was desirable to readily remove the samples if need be or to change the crystals being studied; also, a suitable adhesive capable of withstanding stresses at liquid nitrogen temperatures and with a low vapour pressure, was not available.

2.3.2 Temperature Measurement and Control

The temperature of both samples was monitored by the use of copper-constantan thermocouples which were clamped in contact with each crystal via small heat-conducting copper flanges. The

thermocouples were calibrated against each other to remove bias in the temperature measurements. During the course of the run which lasted from 1 to 2 hours, a time record of the temperature was made approximately every ten minutes and more often if the sample heater was on; calibration tables of temperature in centigrade versus the signal voltage in millivolts had been prepared at one-millivolt interval steps by a five point lagrangian interpolation of commonly available tables (Chemical Rubber Company) and were used in conjuction with a Keithley 160 digital millivoltmeter. Accuracy better than one millivolt was not necessary since deviations of this order were expected although the instrument was properly grounded and shielded. All temperature readings for a run were then reduced to a weighted time average (taken over the period of measurement) which smoothed out small fluctuations and accounted for any time dependent temperature drift (see chapter three for further details).

All thermocouples and heater connections were made to be removable from the sample holder and were fed through to a removable flange equipped with an O-ring vacuum seal. Thus all internal wiring necessitated manipulation only at the time of installation of the sample itself. All external connections were made at the flange lead-ins.

The heating coil, with an approximate resistance of 32 ohms, was controlled by a variac operating on line voltage, and required very little power to achieve a rise in temperature of

the sample. In order to control the temperature during a run, the level of liquid nitrogen in the reservoir was kept constant by a thermistor-pump feedback mechanism. With the thermistor mounted in the reservoir at some depth below the liquid nitrogen surface, a mechanical air pump would be engaged via a relay as soon as the liquid level dropped sufficiently to expose the thermistor to the warmer room air, thereby allowing more liquid nitrogen to be pumped into the reservoir from a large 25 litre dewar.

This method would work quite well after an initial equilibrium period of approximately 45 minutes enabling the temperature to be controlled within plus or minus one degree centigrade without the heating coil being on. However, with it on the equilibrium time was generally longer, and as a result one would observe a weak systematic temperature drift with time, necessitating the use of a weighted time average.

As mentioned previously, fluctuations and drifts in temperature were sufficiently smoothed out by the use of the mild steel heat shunt. Such an element of relatively low thermal conductivity causes a high phase lag in heat flow from the sample holder to the reservoir (providing a 'thermal inertia') so that, after the initial equilibrium period, any gross variations in temperature are damped out somewhat before reaching the sample itself. In this way it was possible to minimize the rate of sample warm-up up to one hour after a sudden depletion of the liquid nitrogen reservoir. The heat shunt was also useful in the reverse case, so that boil-off of liquid nitrogen was minimized

whenever the heating coil was in operation.

2.3.3 Sample Preparation and Mounting

Both samples were of cylindrical shape (13 mm high and 13.6 mm in diameter) and were mounted onto the holder so that when switched into place, the flat face of the sample was normal to the axis of the source holder (see diagram 3). The sample would then receive a large flux of positrons normal to the end face.

The single crystal was obtained from Metals Research Incorporated, England and was unoriented and of 99.999% purity. The single crystal sample itself was trimmed to size by a spark-cutter, a machine specifically designed for the electrostatic cutting of crystalline and fragile materials with minimization of mechanical damage and the introduction of lattice defects.

The polycrystalline sample was prepared and trimmed using zinc of the same purity obtained from Canada Bronze Company Limited (Winnipeg). Both samples were then sealed under vacuum inside quartz tubing and were then carefully annealed at 300° C for approximately 24 hours. The samples were further treated by chemically etching and then polishing all surfaces by using mildly concentrated nitric acid. Immersion times were only brief (approximately two seconds at a time), but the samples were treated repetitively until the surface seemed sufficiently free

of undersirable features and smooth enough to allow channeling and diffraction to occur if indeed they did occur.

As mentioned previously, the sample holder was hexagonal in shape and was modified so that a 60° rotation was possible by a simple mechanical lever connection movable from the top of the upper housing through a sealed extension. This enabled one to switch the sample being studied without any need to dissassemble the entire apparatus allowing both samples to be studied while the system was held at low temperature. A spring loaded click-stop mechanism built onto the sample holder, held the holder securely in one or the other position.

2.4 The Positron Source

The positron source for this experiment was a 15 millicurie Na^{22} source, manufactured by Amersham-Searle (U.K.), and sealed in a glazed ceramic matrix which was mounted in a stainless steel support. The active glaze area itself was rectangular in shape (16 mm by 7.5 mm), fairly thin, and centred within the stainless steel holder which was 32 mm in diameter.

The source sat inside a special holder machined from hard lead, which provided a small degree of collimation of the emitted positrons. The wall of the holder was sufficiently thick enough to block gamma radiation emitted horizontally. The distance of the active glaze area to the crystal face was approximately one centimetre. The proximity to the sample, the thinness of the

source, and the slightly submerged seating of the source within the lead holder, all combine to maximize the number of positrons that are incident normal to the crystal face. The glazed ceramic source proved especially practical since it could be easily subjected to low pressures without giving rise to the problems normally associated with Na^{22} salts used in custom-made sources, and also it could be easily removed without problems when desired.

CHAPTER THREE

ANALYSIS AND TREATMENT OF DATA

3.1 Measurement of Count Rates

If one considers the quantities measured by a conventional long-slit apparatus where one detector is movable, then the observed count rate at a certain angle is given by:

$$(1) \qquad P(\theta) = \int_{-\infty}^{\infty} d\theta' \; \rho(\theta') \; R(\theta - \theta')$$

This represents the convolution of the apparatus' resolution function $R(\theta)$, when the movable detector is situated at some angle θ, with the true annihilation rate $\rho(\theta)$. Previous workers have integrated $P(\theta)$ over the total range available with their geometry. This process is subject to some error, and is somewhat time consuming, as a separate run is required for each incremental step. To observe any temperature effects, run time would be prohibitively long. Therefore, it was the intent of this experiment to measure the integrated or net count rate as a function of temperature by implementing a wide-slit geometry, thus obviating the large time expenditure.

Consider the observed count rate as given by (1) under the conditions that the movable detector is fixed at zero and the opposite detector subtends a much wider angle. Then from (1) we have:

$$(2) \qquad P(o) = \int_{-\infty}^{\infty} d\theta' \; \rho(\theta') \; R(\theta')$$

This quantity, as it stands, would have little meaning by itself, were it not for the fundamental difference in the resolution function introduced by the wide-slit geometry. As we shall see (2) represents a net integration of $\rho(\theta)$ over a sufficiently large range of angle to make it useful in the context of this experiment.

3.1.1 The Wide-Slit Resolution Function

The typical resolution of the conventional apparatus is of the order of a milliradian so that the count rate expressed by (1) or (2) gives us only approximate knowledge of $\rho(\theta)$, unless the resolution function is known, in which case a deconvolution can be performed (also with its own accompanying errors). The resolution function is not only a function of the geometry, but also of the effective sample size as seen by the detectors, and of the penetration depth of positrons into the sample and can be, as a result, quite complex in shape to describe analytically.

The approach taken to compute the resolution function for the wide-slit geometry was semi-analytical in nature, using the known parameters and restrictions of the system to specify a computer algorithm by which the resolution function could be found (see Appendix II for a complete discussion). The algorithm is essentially a 'hit or miss' Monte-Carlo application and takes

into consideration the finite shape and size of the sample. Figure 1 shows the results of a run done for the exact specifications of the system. Several other runs were also done with varying sample sizes and it was found that the results were fairly insensitive to such changes.

Looking at figure 1, two prominent features crop up:

a) the resolution function has an extremely large F.W.H.M. of the order of the angle subtended by the wide-slit and

b) the shape of the resolution curve is very flat resembling a square step function, and falls off rapidly beyond the half-maximum point.

With this in mind, the measured quantity given by (2) becomes:

$$(3) \qquad P(0) \simeq A \int_{-\theta_F}^{\theta_F} d\theta \, \rho(\theta) \qquad + O\left(\frac{d}{d\theta} \rho(\theta_F) \right)$$

where $2\theta_F$ is the F.W.H.M. of the resolution curve (θ_F is approximately 25 mrad for the geometry used.). Since $R(\theta)$ falls off rapidly beyond θ_F and the tail of $\rho(\theta)$ is monotone decreasing, the relative error that one may incur is small (see appendix II). Collimation of the sample to reduce the effective sample size as seen by the detectors, was not done, since this had only the effect of reducing the F.W.H.M. by an order of δ, the ratio of sample radius to the distance between the sample and the narrow detector (see Appendix II). This effect did not seem advantageous in the context of this experiment.

Figure 1

Wide-Slit Apparatus Resolution Function

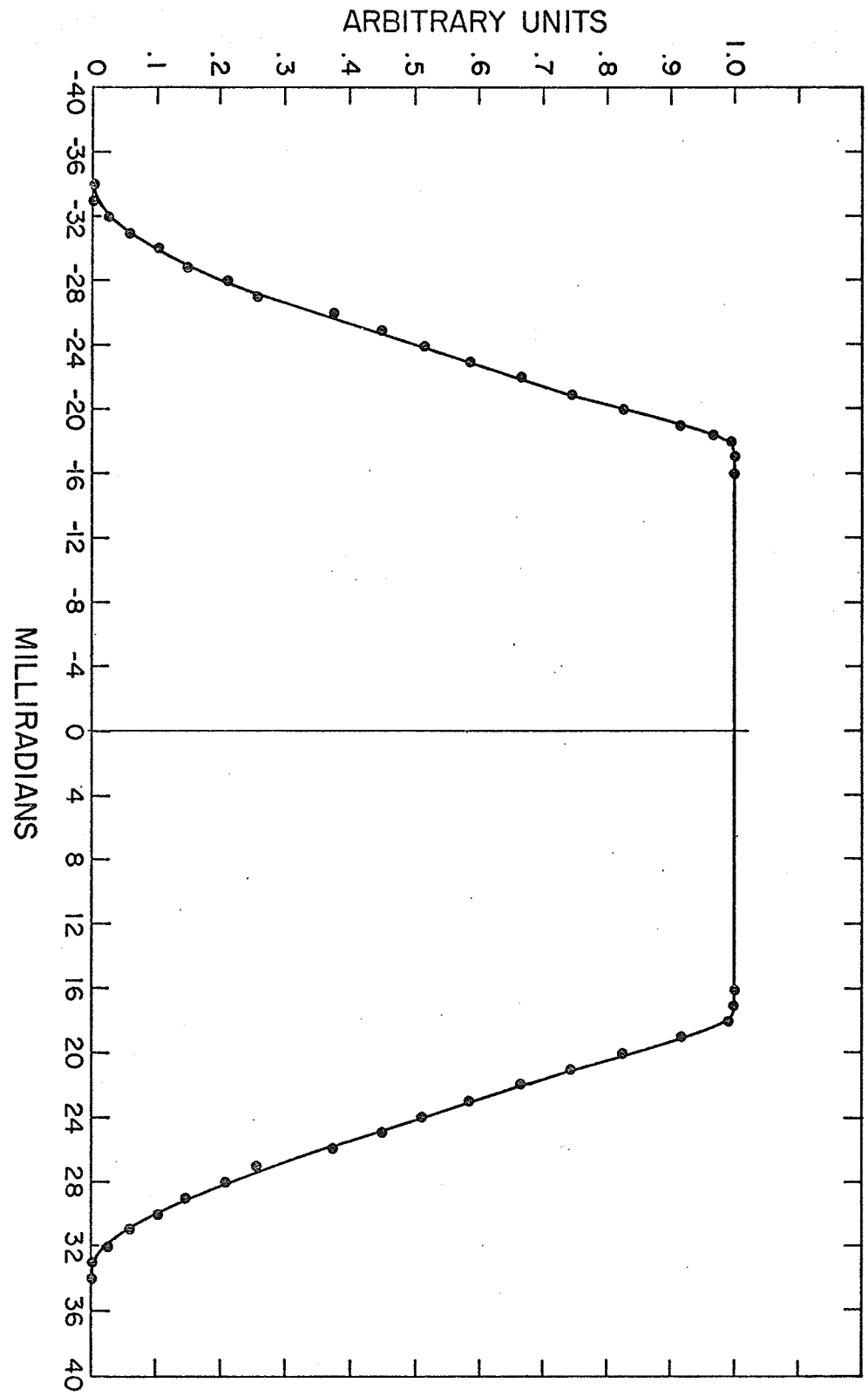
ARBITRARY UNITS
0
.1
.2
.3
.4
.5
.6
.7
.8
.9
1.0
MILLIRADIANS
-40
-36
-32
-28
-24
-20
-16
-12
-8
-4
0
4
8
12
16
20
24
28
32
36
40

3.1.2 Counting Statistics

We shall refer to (3) as the integrated count rate. It is commonly known that observations of the number of events occurring during a time interval Δt when the probability of occurrence is considered small, follows the Poisson process; defined by:

a) $\Pr\ (n=1 \mid t' \leqslant t \leqslant t'+\Delta t) = \lambda t + \mathcal{O}(\Delta t^2)$

b) $\Pr\ (n\ 1 \mid t' \leqslant t \leqslant t'+\Delta t) = 0 + \mathcal{O}(\Delta t^2)$

c) $\Pr\ (n=0 \mid t' \leqslant t \leqslant t'+\Delta t) = (1-\lambda t) + \mathcal{O}(\Delta t^2)$

where λ is a proportionality constant or a probability rate.

Thus, events which follow this process will have the poisson distribution:

$$(4) \qquad \Pr(N=n;t) = ((\lambda t)^n/n!)\ e^{-\lambda t}$$

(4) gives the probability of getting exactly n events occurring in a time of measurement t. Then the mean number of events in a time t is:

$$(5) \qquad \langle N \rangle = \lambda t$$

It is also a property of (4) that the variance is given by:

$$(6) \qquad \sigma^2(N) = \langle N \rangle = \lambda t$$

An unbiased estimator for the probability rate (or count rate) is given by :

$$(7) \qquad \hat{\lambda} = \langle N \rangle / t$$

It must be kept in mind that $\hat{\lambda}$ is the directly observed integrated count rate (3). Then the relative error in $\hat{\lambda}$ in terms of the standard deviation is given by:

$$(8) \qquad \Delta\hat{\lambda} / \hat{\lambda} = \sigma(N) / \langle N \rangle = 1/N^{1/2}$$

Typical run times were of the order one to two hours, so that the total accumulated count in that time was generally 40,000, giving relative errors less than ½%. The time interval as measured by the timer was accurate to within 0.10 seconds, so that the statistical errors outweigh the timing errors. Some runs of much longer duration were also made, but temperature control over longer periods became increasingly more difficult when the sample heater was employed.

In order to monitor the chance coincidence rate for each run, the count rate from each detector (the 'singles' count rate) was measured before and after a run. Then, using the value for the resolution time τ of the coincidence circuit, the chance coincidence rate P_{cc} was estimated from equation (1) of Chapter 2:

$$(9) \qquad P_{cc} = 2\tau P_1 P_2$$

where P_1, P_2 are the singles count rates. The values obtained were of use in measuring the proportion of true coincidences occurring in each measurement, and provided a means of checking whether results were consistent from run to run.

3.2 Temperature Measurements

Using the method described in Chapter 2 to control the temperature of the samples during a run, the time to reach equilibrium from room temperature was on the average about 45 minutes. Once having attained this temperature, the heater coil could be engaged to raise the sample temperature, thus requiring an additional 30 minutes to stabilize.

During a run, temperature measurements were made every 5 minutes or so using the digital millivolt-meter to read the thermocouple signals. As mentioned previously, the thermocouple calibration tables were prepared at 1 mv intervals from -200°C to 100° C from published tables (Chemical Rubber Company) by using a step by step Langrangian interpolation formula employing five tabulated points for each step interpolation (see page 42, Ralston - Numerical Analysis).

The need to monitor the temperature with such frequency, was necessary to extract a mean temperature for the run, and

eliminate the small fluctuations about the mean that were unavoidably present. Little difficulty was experienced when the heater coil was not on; however, the heater did extend the equilibrium time required so that some small component of temperature drift with time was anticipated.

In order to surmount the problems of both the stochastic fluctuations and the systematic drift, a weighted time average of the temperature was obtained from an integration over the run time using a generalized unequal-interval trapezoidal rule as follows:

$$(10) \quad \langle T \rangle = 1/t_R \sum_{i=o}^{n} \Delta t_i \, T_i$$

where the Δt_i are evident from the expansion:

$$\langle T \rangle = 1/t_R \; [.5 \; T_o (t_1 - t_o) + .5 \; T_1 (t_2 - t_o) + \ldots$$
$$\ldots + .5 \; T_{n-1} (t_n - t_{n-2}) + .5 \; T_n \; (t_n - t_{n-1}) \;]$$

Similarly:

$$(11) \quad \langle T \rangle = 1/t_R \sum_{i=o}^{n} \Delta t_i \langle T_i^2 \rangle$$

(private communication, Dr. A.N. Arnason, Department of Computer Science, University of Manitoba)

from which we can also obtain an estimate of the variance:

$$(12) \quad S^2(T) = \langle T^2 \rangle - \langle T \rangle^2$$

Values of S were typically of the order of 1.8 C° and are reported alongside of values of $\langle T \rangle$ in Table 1.

3.3 The Experimental Data

Table 1 shows the measured integrated count rates for both the polycrystalline and single-crystal samples versus their respective mean temperatures as given by (10). The associated standard deviations for the count rates and the mean temperatures, as given by (8) and (12) respectively, are also included.

It should be mentioned at this point, that although electronic drift of the apparatus was no problem during a run or even during the course of one day, it was noticeable over a period of several days. For this reason, if the apparatus had been idle for several days, the next run was augmented by a reference run at room temperature. Since the only parameters of the system that had been changed in the interval were the electronics, due to drift, the reference run results could be correlated to previous reference runs at room temperature. Changes in the electronics due to drift could also be monitored through the measurement of the chance coincidence count rates.

Diagrams 2 and 3 show the data of Table 1 plotted without any changes. Note that in each diagram, an attempt has been made to show the general trend of the data. This was done by a linear 'least-squares' fit for the region below room temperature for

TABLE 1

Poly Crystalline Sample		Single Crystal Sample	
Temperature C	Integrated Count Rate P(0)	Temperature C	Integrated Count Rate P(0)
136.79 ± 2.70	795.27 ± 3.42	108.11 ± 1.40	709.78 ± 3.41
116.67 ± 6.1	793.71 ± 3.29	97.23 ± 2.90	711.69 ± 3.52
90.22 ± 2.95	794.23 ± 3.53	82.67 ± 3.95	711.10 ± 3.20
46.91 ± 1.10	795.23 ± 3.54	54.71 ± 0.32	712.15 ± 3.54
18.15 ± 3.04	793.72 ± 3.85	17.92 ± 0.45	709.51 ± 3.52
-28.28 ± 2.0	791.17 ± 3.61	-16.49 ± 0.19	704.64 ± 3.30
-44.05 ± 0.49	789.68 ± 3.61	-29.87 ± 1.30	701.12 ± 3.31
-68.13 ± 0.22	788.85 ± 3.76	-33.48 ± 2.10	701.72 ± 3.48
-87.51 ± 0.17	787.85 ± 3.70	-46.11 ± 1.60	699.80 ± 3.35
		-78.25 ± 2.80	693.32 ± 2.48
		-81.01 ± 0.17	693.91 ± 3.29

Figure 2

Temperature Dependence of Count Rates

for Poly-Crystalline Zinc Sample

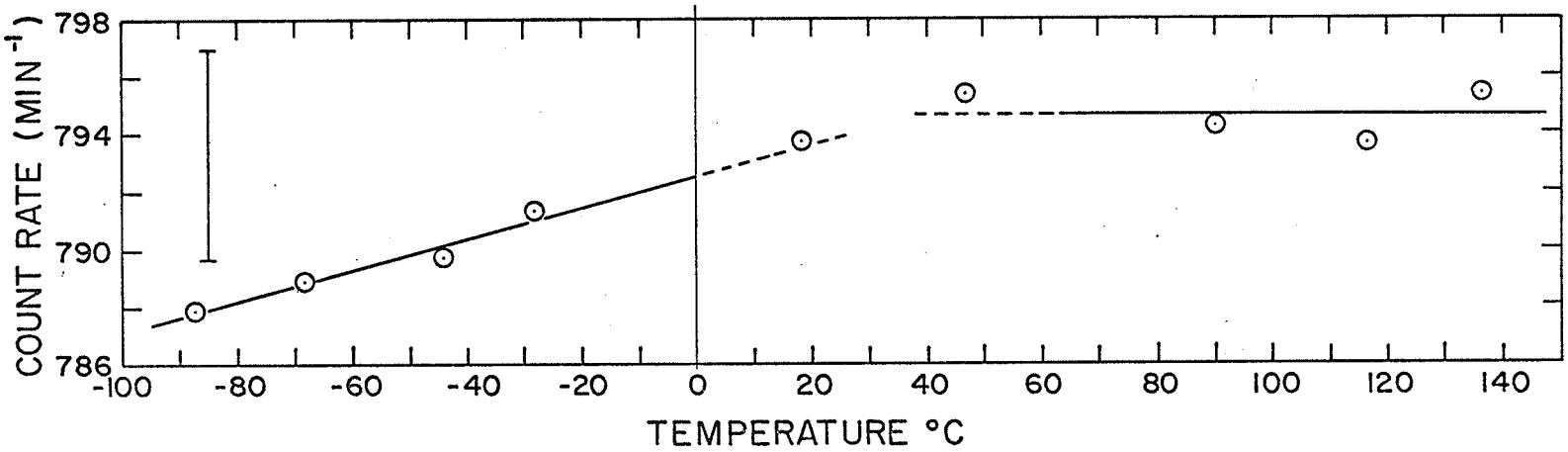
COUNT RATE (MIN⁻¹)
798
794
790
786
-100
-80
-60
-40
-20
0
20
40
60
80
100
120
140
TEMPERATURE °C

Figure 3

Temperature Dependence of Count Rates for Single Crystal Sample

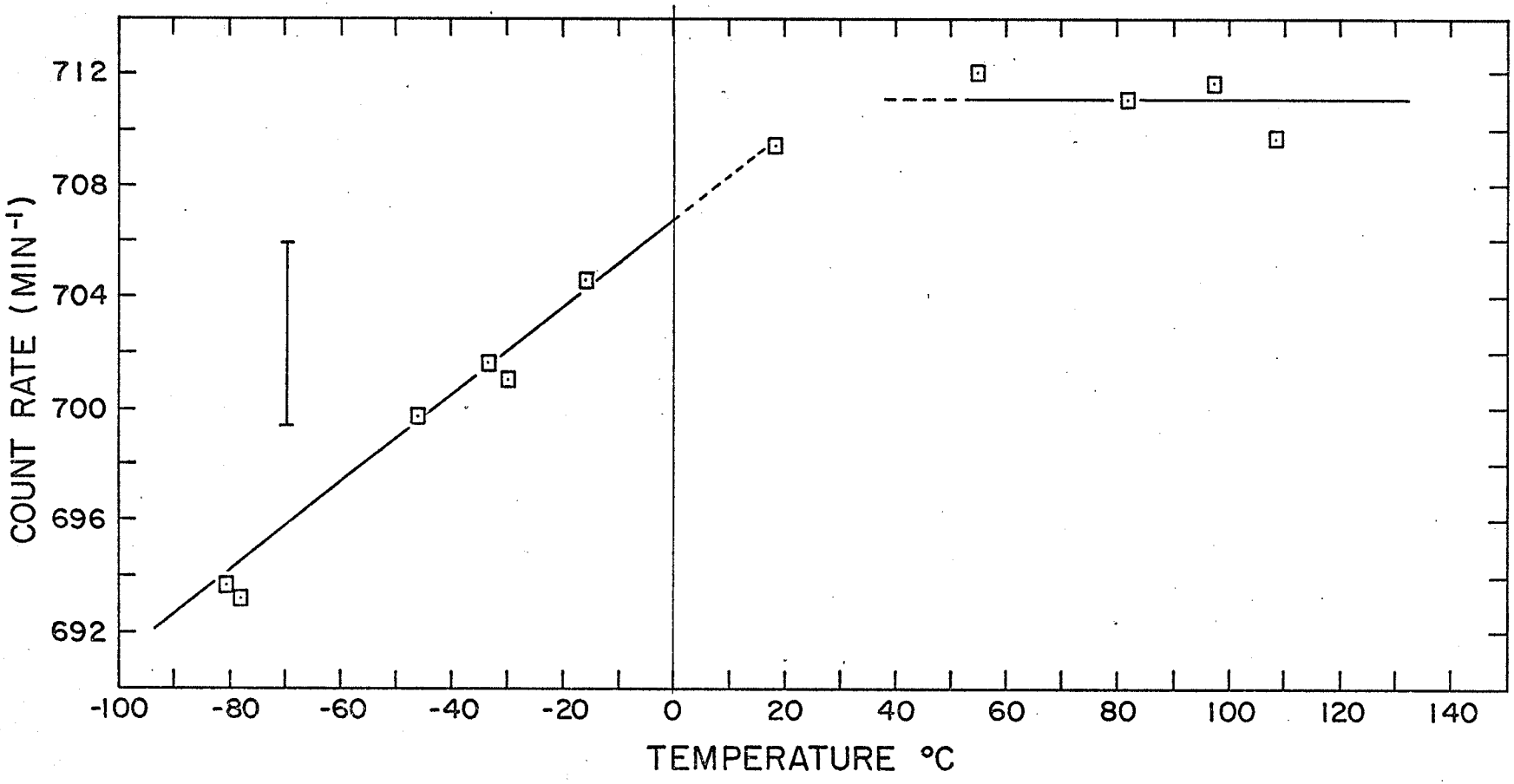
712
708
704
700
696
692
COUNT RATE (MIN-1)
-100
-80
-60
-40
-20
0
20
40
60
80
100
120
140
TEMPERATURE °C

Figure 4

Data for Single and Poly Crystal Samples

Normalized to a Common High Temperature Limit

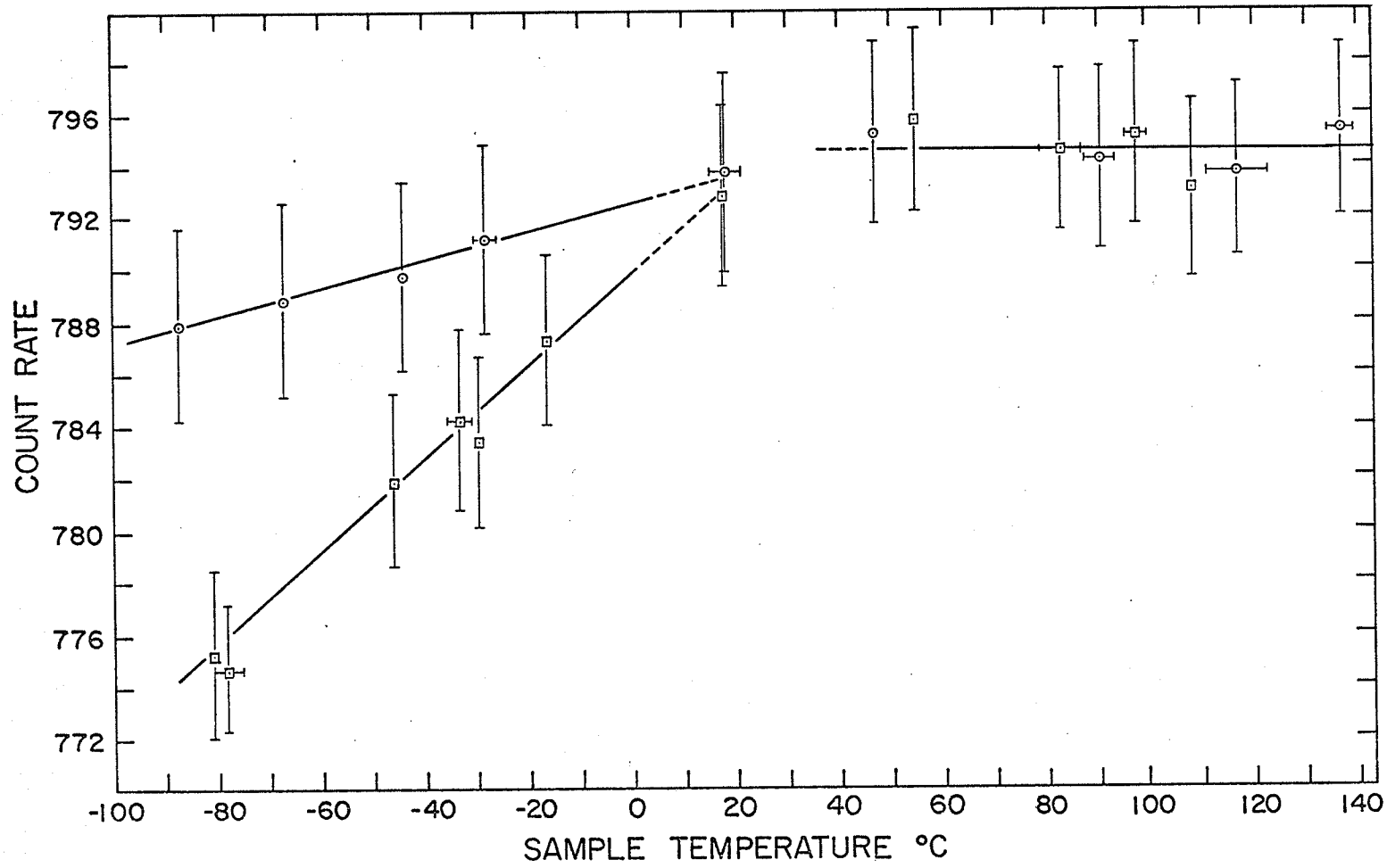
796
792
788
784
780
776
772
COUNT RATE
-100
-80
-60
-40
-20
0
20
40
60
80
100
120
140
SAMPLE TEMPERATURE °C

both cases; however, for the region above room temperature, the horizontal line represents the mean count rate over that region, reflecting a basic assumption that any temperature effect that may exist in either sample, will eventually diminish in strength as the temperature is raised above room temperature. This will be discussed in further detail in the next chapter.

Diagram 4 is shown here for completeness, but full interpretation is left until the next chapter. Essentially, the single crystal data has been 'normalized' to that of the polycrystalline sample, so that the behaviour of one, at high temperatures, becomes asymptotically indistinguishable from that of the other (with respect to the different hypothesized mechanisms that are treated in the discussion to follow).

CHAPTER FOUR

DISCUSSION AND CONCLUSION

4.1 Features of Results

In attempting to analyse and interpret the results of the experiment as shown in the last chapter, it is helpful to refer back to the history of previous research work that has been done and which was briefly outlined in section 1.5.

Turning to the results as they stand in section 3.2, we see that there are three basic outstanding features that require investigation. First of all, and probably the most important is the definite systematic difference between the count rates for the two samples (figures 3-2, 3-3 and 3-4) as the temperature is lowered below room temperature, the single crystal showing a more pronounced dependence upon the temperature. The differences in the normalized count rates (figure 3-4) at the lowest temperature observed is approximately 1.6% as compared to the standard errors which are less than 0.5%.

Secondly, as one raises the temperature above 300° K the temperature dependence in both samples effectively disappears, and any finer structure in the data is swamped by the statistical errors. Finally, from table 1 one can see that, even for temperatures above 300° K, that the count rates for the polycrystalline sample are approximately 11.7% higher than that of the single crystal. This last effect cannot be attributed to a

variation of the solid angle subtended by the sample face, as seen from the source, since the differences in dimensions would produce a net change of approximately only 1%.

In regard to the other effects observed, one notes that any temperature effect due to:

a) the source itself

b) the source-sample housing

c) ice formation on samples in the case of an imperfect vacuum

d) sample shrinkage (the differences in the solid angle subtended as mentioned above are negligible with respect to the differences observed)

would contribute equally to both samples observed. Similarly, no systematic variation of the electronics could account for these effects, since the order of the runs was random with respect to time and temperature; also the same electronics were used for both samples and any variations were monitored through the use of the 'singles' count rates.

It would seem then that the effects observed arise from a definite physical process. One might also note that the Debye temperature of zinc is approximately 308° K, (C.Kittel, Introduction to Solid State Physics) which corresponds roughly to the break in the temperature dependences observed for both samples.

4.2 Discussion

Possible candidates for the mechanism by which these temperature effects may arise were discussed in chapter 1, and those that have been unresolved to this date are:

a) channeling of positrons into the crystal

b) diffraction of positrons off the face of the crystal or into the interior of the crystal

c) diffraction of positrons at some depth in the crystal and a subsequent channeling exit

d) non-thermalization in the ordered structure of the single crystal.

and some combination of these might take an active role in producing the effect. We shall consider each separately, and discuss their validity in light of the results of this and previous works.

4.2.1 Non-Thermalization

As mentioned in chapter 1, Carbotte and Arrora (1967), have produced calculations that suggest that the thermalization time may be somewhat longer than the annihilation lifetime in metals at low temperatures. If this is the case, annihilation in flight would yield counts appearing at higher momentum, thus depleting the observed counts at low momentum. Furthermore the

effect increases with decreasing temperature, eventually vanishing when the thermalization time is lower than the annihilation lifetime. The calculations do not reflect any ordered structure so that one expects an identical effect in both samples. However since the high disorder and presence of grain boundaries and possible vacancies in the poly-crystal will certainly increase the amount of scattering of the positron, the thermalization time is on the average shorter and the effect may be somewhat diminished or absent altogether in the poly-crystal (compare with figure 3-4).

4.2.2 Channeling

We shall consider two variations of possible channeling mechanisms (positron channeling has been observed for some time in thin samples. See Andersen et al, 1971, Walker et al, 1970 and Vorobev et al, 1971)

a) Channeling into the crystal and subsequent annihilation in the interior of the crystal.

Present indications show that the penetration range of channeled particles having energy of the order 0.1 to 0.5 Mev would be of the order of 800 microns or less (Davies et al, 1967, Erickson, 1968 -using ^{42}K in tungsten). This is an order of magnitude estimate, since the range of the particle depends on

both its energy and the incident angle upon entry into the channel. If the entry angle is too close to the critical angle of acceptance (Lindhard, 1965), dechanneling may occur within a relatively short distance due to multiple scattering. It is for this reason that most channeling researchers to date have used extremely thin (1 micron or less) single crystals.

With this in mind, annihilation in flight, during channeling, would have the same consequences as the non-thermalization discussed above, those being a change in shape of the momentum distribution and a drop in low momentum peak. In the channeling case, it has been found that the channeling efficiency rises with decreasing temperature below the Debye temperature (Davis et al, 1967; Vorobev, 1971). Thus the shift to higher momentum components would increase with decreasing temperature.

One must also note, however, that since the efficiency of the channeling is temperature dependent, that the transmission efficiency of incident positrons into the sample also increases with decreasing temperature. Thus, the total number of possible annihilations must increase with decreasing temperature; this is a trend counter-productive to the annihilation in flight mechanism, so that the net effect may indeed be small.

Furthermore, although the results of past workers (and those of this work also) show a drop in the count rates integrated over the range of their equipment (Faraci, 1969, 1970(b); Dekhtyar 1961, 1969), Faraci et al did not find any

change in shape over the range measured (0-10 mrad).

In addition, annihilation in flight, requires that the annihilation lifetime be much shorter than the dechanneling time; however, for the energy spectrum of Na^{22}, and for the penetration range given above, we find that the dechanneling time is of the order 10^{-12} sec which is much shorter than the lifetime in metals ($\sim 10^{-10}$ sec). This seems to be a contradiction, or the actual penetration ranges of channeled positrons is much longer. However, dechanneling increases proportionately to the range (Davies et al, 1967; Andersen 1971). In retrospect, annihilation in channeled flight seems to be an uncertain and perhaps improbable cause for the effect.

Consider then, the case where the dechanneling time is less than the annihilation time (note that 10^{-12} sec is also the theoretical value for thermalization times). No residual momentum would be present with no consequent shift in the momentum distribution. Then the only possible temperature dependent effect would be the increase in total number of annihilations due to the increase of transmission efficiency. This would give rise to an increase in integrated count rate contrary to what has been observed in this work and elsewhere.

b) Channeling with Subsequent Exit from the Crystal.

If we assume that it were possible for the penetration of channeled positrons to be large enough that they subsequently

exited from the crystal altogether and annihilated outside of the range of possible detection by the apparatus, then one would expect not only a drop in the net integrated count rate but also observe no change in shape of the distribution. Furthermore, as the temperature is dropped, the channeling efficiency increases, and the effect also increases. This would certainly be in agreement with the results to this date, however, as has been mentioned above, the range or penetration of the channeled positrons does not seem likely to be large enough to allow complete exit from large bulk crystals as have been used in this and previous experiments.

It is important to mention at this point that Faraci et al (1970a) designed an experiment to detect escaping positrons from a single crystal of lead. The 'thin' crystal used was cylindrical in shape and hollow to contain a Na^{22} source. This entire sample-source arrangement was encapsulated in Teflon. If positrons escaped the lead crystal then the very long lifetime component of annihilations in Teflon superimposed upon the time spectra of lead would give positive confirmation (B. G. Hogg et al 1968), as well as show a change as the temperature changed. No such Teflon tail was observed within the experimental error, as well as no temperature dependence. The stated conclusion was that exit due to channeling was rare, if not absent. It should be kept in mind however that for the lead crystal used the dimensions were not specified. It may have been too thick altogether and complete penetration not possible. At best the

results are only inconclusive.

4.2.3 Diffraction of Positrons

a) Diffraction off surface of crystal.

For diffraction of positrons off the face of the crystal, the diffraction intensity would increase as the temperature drops below the Debye temperature, resulting in a decrease of the transmitted number of positrons. Those that are transmitted, are not altered in their momentum and thus the net consequence would be a decrease in integrated count rate and no change in shape as the temperature is dropped. This again would fit the observations. Of course, the poly-crystal, being highly disordered, would exhibit little or no effect. Previous workers have observed no effects in the poly-crystals, within experimental error, and the errors present for the data of this work would also put the slight trend of the poly-crystalline data in question.

Furthermore, Dekhtyar, in an experiment to detect possible diffraction off the crystal face of a zinc crystal quotes in the text of his paper a 7% drop in integrated count rate, while unfortunately the graphs in the same paper indicate a 7% rise which would contradict the diffraction hypothesis and support the channeling hypothesis. From the geometry of the experiment it is possible that what was measured was the

back-scattering rather than diffractionally reflected positrons. This is a somewhat confusing error, and if his basic statement is correct, then the diffraction mechanism is the most likely candidate for the temperature effect. The Teflon lifetime experiment of Faraci et al, as previously mentioned, cannot be expected to have yielded a definite indication of diffraction.

Diffraction off the face of the crystal may also have some bearing upon the 12% net difference in poly and single crystal count rates that was discussed previously (figures 3-2 and 3-3), since relative changes in the solid angle failed to account for the difference.

b) Diffraction into the crystal.

If we consider a fraction of the incident positrons to be diffracted into the crystal rather than off the face, the subsequent consequences are similar to those discussed for the direct channeling process (increasing net integrated count rate with decreasing temperature). Again if it were possible for the positron to annihilate in flight, (non-thermalized) one would expect to see some changes in the shape of the momentum distribution due to Bragg reflection of the positrons. These changes would be orientation dependent as well as temperature dependent. However, such a mechanism results in effects which are not observed in this and previous works. This may be due to the orientation of the sample.

4.2.4 Diffraction into Crystal and Subsequent Exit by Channeling

Dekhtyar originally proposed that positrons entering the sample may be diffracted into a direction favourable for subsequent channeling and final ejection from the crystal with annihilation occurring outside the range of the detectors. Since the efficiency of both the diffraction and channeling mechanisms increase when the temperature is lowered below the Debye temperature, the net effect would be to see the integrated count rate drop with decreasing temperature and no changes in the shape of the momentum distribution. This again would agree with the observed results (not to mention the agreement with results for the poly-crystal sample also); however, as mentioned above the channeling range may be too small to permit such occurrences. The Teflon lifetime experiment of Faraci et al, as discussed above, was unable to clarify whether any mechanism allowing the escape of positrons from the crystal really exists.

It is also of interest to mention the work of Campbell et al(1972) who observed the energy spectra of the 511 Kev annihilation gamma-rays for several metals prepared in both single and poly-crystalline samples. Their resolution was approximately 1.5 Kev using GeLi equipment which corresponds to twice the angular integration range of this work. Working on the premise that enhanced annihilation in flight, due to one of the processes discussed above, would give rise to a higher energy

component and thus deplete the intensity of the 511 Kev peak, they basically found a net positive change with a decrease in temperature of the the order of 1 to 3% with a standard error also of the same order. They then conclude that any of the previously proposed effects must be very small, and certainly smaller than reported by previous workers. The fact that their observed changes were positive in sign contradicts the results of this and previous works, but may support channeling or diffraction into the crystal with subsequent thermalization and then annihilation.

4.3 Conclusions

One must conclude, from the results of this experiment, and taking into consideration the results of previous workers and the possible mechanisms that may take place, that the temperature effect arises most probably from the diffraction of positrons off the crystal face, but that diffraction into a channel and subsequent exit from the crystal may also be possible but less likely because of the confined channeling range. Annihilation in flight does not seem to be the case, nor enhanced transmission of positrons into the sample by channeling or diffraction.

There is a strong need for further penetration range studies of positron channeling. Such basic experiments as Dekhytar's to detect diffracted positrons and Faraci's Teflon lifetime experiment need to be repeated under more controlled

circumstances and with some basic redesign of method. This present work has been successful in that it has confirmed qualitatively the results of both Dekhtyar and Faraci but has found, as did Campbell et al, that the effects are of lesser magnitude than previously thought.

This work has determined a drop in integrated count rate of 2.41% ± 0.66% for the single crystalline sample of zinc and a drop of 0.72% ± 0.66% for the poly-crystalline sample, in going from 293 ^{o}K to 185.5 ^{o}K (well below the Debye temperature for zinc). No such changes within experimental error, have been observed above 300^{o}K.

APPENDIX I

Derivation of Electron-Positron Pair Momentum from the Angular Correlation of 2-Gamma Annihilation Radiation

Let us suppose that the positron is thermalized in the medium and that the electron with which it annihilates by 2-gamma radiation has velocity V. In the lab frame, we may write the conservation laws as:

(1) $m\vec{V} = \vec{p}_1 + \vec{p}_2$; (conservation of momentum)

(2) $\frac{1}{2}mV^2 + 2mc^2 = p_1 c + p_2 c$; (conservation of energy)

where $\vec{p}_1$ and $\vec{p}_2$ are the respective momenta of the gamma rays and $2mc^2$ is the rest energy of the $e^+ - e^-$ pair.

Let us formulate the problem in C.M. coordinates, letting:

$\mu = m/2$	be the reduced mass of the system,
$\vec{V}_c = \vec{V}/2$	be the centre of mass velocity,
$\vec{v}_1$, $\vec{v}_1'$	be the velocity of the e^+ in the lab and C.M. coordinates respectively,
$\vec{u}=\vec{v}_2 - \vec{v}_1$	be the relative velocity in the lab frame.

Then we have:

$$(3)\quad \vec{v}_2 = \mu/m_2\,\vec{u}+\vec{V}_c \quad ; \quad (4)\quad \vec{v}_1 = -\mu/m_1\,\vec{u} + \vec{V}_c$$

$$(5)\quad \vec{v}_2' = \mu/m_2\,\vec{u} \quad ; \quad (6)\quad \vec{v}_1' = -\mu/m_1\,\vec{u}$$

Using these, (1) and (2) become in the C.M. frame,

$$(1)'\quad \vec{p}_1' + \vec{p}_2' = 0 \quad (\therefore \vec{p}_1' = -\vec{p}_2' \text{ and } p_1' = p_2')$$

$$(2)'\quad p_1' c + p_2' c = 2mc^2 + \tfrac{1}{2}\mu u'^2$$

and the two γ-rays are collinear but 180° apart. Now we find in fact that:

$$\vec{u}' = \vec{u} = 2\vec{V}_c \qquad (\text{since } \mu = \tfrac{1}{2}m)$$

Therefore we have:

$$2p_{1,2}' c = 2mc^2 + mV_c^2$$

$$T_\gamma^{C.M.} = p'c = mc^2\left(1 + \tfrac{1}{2}V_c^2/c^2\right)$$

Thus we find that the energies and momenta are of equal magnitude in the C.M. frame. Since, in solving for the momenta, there remains one degree of freedom unspecified, let us allow the scattering angle in the C.M. frame to be some value Φ, (see figure 3, chapter 1) with respect to the incident direction. Then in the lab frame, θ_1 and θ_2 specify the scattering angles for gamma rays #1 and #2 respectively. We will now solve for θ_1 and θ_2.

Now from equations (3) to (6), we can transform back to the unprimed system; however, the equations as they stand do not

hold for relativistic velocities. We see that v_1' and v_2' must be equal to c, and are measured relative to the C.M., which in turn has velocity $\vec{V}_c$ relative to the lab frame. Thus, to obtain valid relativistic values for $\vec{v}_1$ and $\vec{v}_2$ (measured w.r.t. the lab frame) we must apply the Lorentz transformation given by:

$$\mathcal{L} \equiv \begin{bmatrix} \gamma & 0 & 0 & i\beta\gamma \\ 0 & 1 & 0 & 0 \\ 0 & 0 & 1 & 0 \\ -i\beta\gamma & 0 & 0 & \gamma \end{bmatrix} \qquad \text{where} \quad \beta \equiv (V_c/c)$$

$$\text{and} \quad \gamma \equiv [1-\beta^2]^{-1/2}$$

If we apply this to an arbitrary velocity vector $\vec{V}$, we obtain:

$$V_x' = \frac{V_x + V_c}{1 + 1/c^2\, V_x V_c} \quad ; \quad V_y' = \frac{V_y \sqrt{1-\beta^2}}{1 + 1/c^2\, V_x V_c} \quad ;$$

$$V_z' = \frac{V_z \sqrt{1-\beta^2}}{1 + 1/c^2\, V_x V_c}$$

Applying these transformations to equations (3) to (6), we obtain:

$$V_1 \cos\theta_1 = \frac{(\mu/m_1)\, u' \cos\Phi + (V_c/c)}{1 + 1/2 \cos\Phi \cdot (V_c/c)}$$

Since the photons have speed c we have;

$$\cos\theta_1 = \frac{1/2 \cos\Phi + (V_c/c)}{1 + 1/2 \cos\Phi \cdot (V_c/c)}$$

Similarly

$$\sin\theta_1 = \frac{1/2 \sin\Phi \sqrt{1-(V_c/c)^2}}{1 + 1/2 \cos\Phi\, (V_c/c)}$$

Thus:

$$\cot\theta_1 = \frac{\cos\Phi + 2(V_c/c)}{\sin\Phi\sqrt{(1-V_c^2/c^2)}}$$

This, so far, is exact. If $V_c << c$, we then have, to first order:

$$\cot\theta_1 \simeq \frac{\cos\Phi + 2(V_c/c)}{\sin\Phi} + \mathcal{O}(V_c^2/c^2)$$

Thus we see that for $\Phi = 90°$, the deviation from 180° collinearity in the lab frame, is equal to $2(V_c/c.)$ (or V/c for the electron only) to within an order of $(V_c/c)^2$.

We shall also show that the gamma rays energies differ by the same order of magnitude in the lab frame. We have, in the lab frame from (2):

$$P_1 + P_2 = 2mc\,(1 + V_c^2/c^2)$$

and from (1):

$$P_1 \sin\theta_1 - P_2 \sin\theta_2 = 0$$

Thus we find:

$$P_1 = \frac{2mc\,(1 + V_c^2/c^2)}{1 + \sin\theta_1/\sin\theta_2} \quad ; \quad P_2 = \frac{\sin\theta_1}{\sin\theta_2}\cdot P_1$$

From the results of the Lorentz transformation applied to equations (3) to (6) we also have:

$$c\cdot\sin\theta_1 = \frac{c\cdot\sin\Phi\sqrt{(1-V_c^2/c^2)}}{(1 - V_c/c\cos\Phi)} \quad ; \quad c\cdot\sin\theta_2 = \frac{c\cdot\sin\Phi\sqrt{(1-V_c^2/c^2)}}{(1 + V_c/c\cos\Phi)}$$

We finally have that:

$$P_1 c = mc^2 (1 + V_c^2/c^2) \cdot (1 + \cos \Phi \cdot V_c/c)$$

$$P_2 c = mc^2 (1 + V_c^2/c^2) \cdot (1 - \cos \Phi \cdot V_c/c)$$

and thus:

$$\Delta E_{1,2} = 2mc^2 (1 + V_c^2/c^2) \cdot \cos \Phi \cdot (V_c/c)$$

again to first order, this is

$$\Delta E \simeq E_T \cos \Phi \cdot (V_c/c) + \mathcal{O}(V_c^2/c^2)$$

where E_T is the total energy of the system. Then, for $\Phi = 90^\circ$, there is no energy difference, and for $\Phi = 180^\circ$ the difference is approximately $(V_c/c)E_T$.

APPENDIX II

Computation of Resolution Function

The convolution of the true data and the apparatus' resolution function can be written as:

$$(1) \quad P(x) = \int_{-\infty}^{\infty} dx' \; \rho(x-x') \; r(x')$$

where $r(x')$ represents the response of the detector centred at zero angle. Since $\rho(x)$ is a unimodal and symmetric distribution, it is more convenient to consider the equivalent form given by:

$$(2) \quad P(x) = \int_{-\infty}^{\infty} dx' \; r(x-x') \; \rho(x')$$

which gives the count rate when a movable detector is positioned at $x'=x$. For purposes of evaluating $r(x)$, the one detector is considered moveable. Equation (2) corresponds to the geometrical arrangement found in figure 1. We shall now define the quantities shown:

l_1 = distance from sample to narrow slit detector

l_2 = distance from sample to wide slit detector

$2w_1$ = width of narrow slit

$2w_2$ = width of wide slit

x = position of narrow slit (moveable) detector

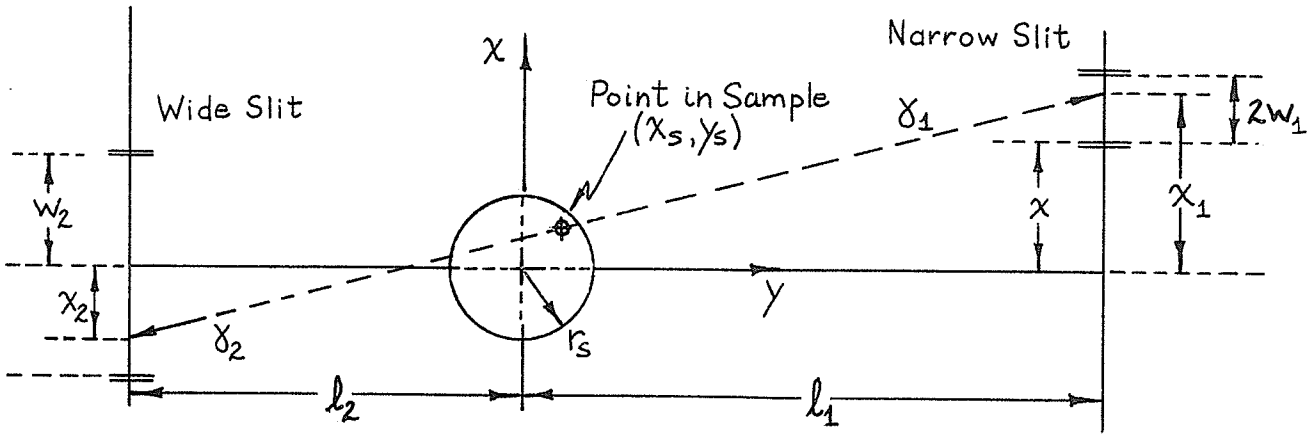

FIGURE 1
(Dimensions are exaggerated)

x_1 = position of gamma ray #1

x_2 = position of gamma ray #2

x_s, y_s = coordinates of annihilation event within the round sample

Note that one can get r(x) directly from (2) if it is known that the annihilation event is prompt and always propagates perfectly anti-collinear gamma rays. This corresponds to:

$$(3) \quad r(x) = \int_{-\infty}^{\infty} dx' \; r(x-x') \; \delta(x')$$

This can be written more formally in terms of the geometrical constraints placed upon the collinear pulses

specified by $\delta(x')$, so that:

$$(4) \quad r(x) = A \int_{-\infty}^{\infty} dx_1 \; H(x,x_1)$$

$$(5) \quad \text{constraint } \mathbb{A} : \quad x-w_1 \leqslant x \leqslant x+w_1$$

$$(6) \quad \text{constraint } \mathbb{B} : \quad -w_2 \leqslant x \leqslant w_2$$

where:

$$(7) \quad H(x,x_1) = \begin{cases} 1 \text{ if } \mathbb{A} \wedge \mathbb{B} = 1 \\ 0 \text{ if } \mathbb{A} \wedge \mathbb{B} = 0 \end{cases}$$

and A is a normalization constant. Equations (5) to (7) define a simple algorithm by which one can compute $r(x)$. Treating x_2 as dependent upon x_s, y_s and x_1 (the independent variables in the algorithm), constraint $\mathbb{B}$ becomes:

$$(8) \quad \mathbb{B} : \left| x_s + (y_s + l_2)\ (x_s - x_1)/(l_1 - y_s) \right| \leqslant w$$

It is more convenient to work in terms of dimension-less quantities. For this reason all quantities are normalized w.r.t. l_1 as follows:

$$(9) \quad \alpha \equiv \frac{l_2}{l_1} \; ; \quad \beta \equiv \frac{w_1}{l_1} \; ; \quad \gamma \equiv \frac{w_2}{l_1}$$

$$\delta \equiv \frac{r_s}{l_1} \; ; \quad \frac{x_s}{l_1}, \frac{y_s}{l_1} \equiv u_1, u_2 \; ; \quad u_4 \equiv \frac{x}{l_1}$$

Now it is possible to construct an algorithm which samples randomly from the 3 degrees of freedom present in $\mathbb{B}$. Let us assume that u_1, u_2 and u_3 have the following uniform distributions:

$$u_3 \sim U[-\beta, \beta]$$

$$u_1, u_2 \sim U[0, \delta] \quad \text{subject to } u_1^2 + u_2^2 \leq \delta^2$$

Then condition $\mathbb{A}$ is automatically satisfied by a random choice of U_3 within $[-\beta, \beta]$ and condition $\mathbb{B}$ becomes:

$$(10)\quad \mathbb{B}: \left| u_1 + (u_2+\alpha)\ (u_1-u_4-u_3)/(1-u_2) \right| \leq \gamma$$

We then proceed to sample, for every step of milliradian angle u_4, randomly from u_1, u_2 and u_3 and count the number of occurrences where the acceptance criterion (10) is satisfied. The programs used are shown in figures 2 and 3. The pseudo-random number generator used is due to P.A.W. Lewis (I.B.M. Systems Journal, 1969) and has been found to have statistical properties superior to previously implemented generators. The generator was written in 360 ASSEMBLER and is shown in figure 3.

Typical results of the program using the specifications of the apparatus were shown in figure 1 of chapter 3.

Accuracy of the method, depends of course, upon the number of samples taken per interval. The number of successes recorded follows a binomial distribution so that the variance in each channel is given by:

$$\sigma^2(x_i) = Np(1-p) = Nr(x_i)\ (1-r(x_i))$$

where N is the total number of trials per channel. Since r(x) is known only approximately we have:

$$\sigma^2(x_i) \simeq n(x_i)\ (1-n(x_i)/N)$$

where $n(x_i)$ is the number of successes recorded in the i'th channel. Then the relative error becomes:

$$(11) \quad \sigma_i / n_i = \frac{1}{n_i^{1/2}} \sqrt{(1 - n_i/N)}$$

Note that this vanishes when $n_i \to N$, and for small n, we have approximate Poisson statistics. Note also that the approximation given by equation 3 of chapter 3,

$$P(o) \simeq A \int_{-\theta_F}^{\theta_F} \rho(\theta)\, d\theta \quad + \mathcal{O}\left[\frac{d}{d\theta} \rho(\theta_F) \right]$$

is valid if $\rho(\theta)$ is a sufficiently smooth function in the sense that all of its successive derivatives vanish as θ tends to infinity and if they are sufficiently small enough for $\theta \gtrsim \theta_F$. This is expected to hold, since $\rho(\theta)$ can be shown to be a proper distribution.

```
C       ALGORITHM TO DETERMINE RESOLUTION FCN.
C
        REAL MRAD(20)
C       MRAD STORES THE OBSERVED FREQUENCY VECTOR. NSAM IS THE NO OF
C       TRIALS PER BOX.SPECIFY PARM''S OF SYSTEM. IOFFST SPECIFYS
C       THE STARTING POSITION IN MILLIRADIANS. IST IS THE RANDOM NO.
C       GENERATOR SEED.
C
        DATA MRAD/20*0./,ALPHA/.529434/,BETA/.2830188E-3/,DELTA/.2566038E-2/,
       @2/,
       *MRADM/020/,NSAM/1000/,X/.50897/,AREA/0./,GAMMA/.013476/,SCALE/1./,
       *IOFFST/30/,PI/3.1415926/,IST/123456789/
        M=MRADM+1
        WRITE(6,8)
      8  FORMAT(16X,'RADIANS',14X,'COUNTS'/)
C
C       REPEAT CYCLE FOR EACH ANGLE GIVEN BY U4.
C
        DO 1 IBOX=1,M
        U4=.001*(IBOX-1+IOFFST)*SCALE
C
C       THIS CYCLE CHOOSES COORDINATES WITHIN THE ROUND SAMPLE AND ALSO
C       THE EXTRA DEGREE OF FREEDOM WITHIN THE SLIT BOUNDARIES, AT RANDOM.
C       A LEWIS PSEUDO-RANDOM NUMBER GENERATOR,WRITTEN IN 360-ASSEMBLER,
C       IS USED.
C
        DO 2 IXS=1,NSAM
        CALL RANDOM(IST,X)
        U3=BETA*(2.*X-1)
      9 CALL RANDOM(IST,X1)
        CALL RANDOM(IST,X2)
        IF(X1*X1+X2*X2.GT.1.) GO TO 9
        U1=DELTA*(2.*X1-1)
        U2=DELTA*(2.*X2-1)
C
C       EVALUATE THE ACCEPTANCE CRITERION OF  THE OTHER SLIT (EVALF).
C       DETERMINE IF THE TRIAL IS ACCEPTED OR NOT.IF ACCEPTED, INCREMENT
C       THE BOX COUNTER.
C
        EVALF=ABS(U1+(ALPHA+U2)/(1.-U2)*(U1-U3-U4))
        IF(EVALF.LE.GAMMA) MRAD(IBOX)=MRAD(IBOX)+1.000
      2 CONTINUE
C
C       KEEP TALLY ON THE TOTAL NO. OF ACCEPTED COUNTS AND PROCEED TO
C       NEXT ANGLE.
C
        AREA=AREA+MRAD(IBOX)
      1  WRITE(6,6) U4,MRAD(IBOX)
C       OUTPUT THE RESULTS AND  A HISTOGRAM (HIST - FROM IBM S.S.P)
        WRITE(6,7) AREA
      7 FORMAT(10X,'TOTAL AREA OF RESOLUTION CURVE = ',1F15.8/)
        CALL HIST(1,MRAD,20)
      6  FORMAT(10X,2F15.8)
        END
```

Figure 3


```
RANDOM   CSECT     LEWIS GENERATOR - CALL RANDOM(IST,X) - FOR WATFIV
         USING RANDOM,15
         STM 1,12,12(13)      SAVE WATFIV REGISTERS
         LM 2,3,0(1)    LOAD ARGUMENT ADDRESSES FROMR1 INTO R2,R3
         L 5,A
         M 4,0(2)     MULTIPLY A BY IST ARG
         D 4,P     DIVIDE THE RESULT BY 2**31-1
         ST 4,0(2)    STORE IT IN IST ARG
* SET UP A REAL*4 FOR THE 2ND ARG
         SRL 4,7 MAKE ROOM FOR EXPONENT
         A 4,CHAR    PUT IN EXP
         ST 4,0(3)  PASS RESULT TO ARG2
         LM 1,12,12(13)    RETURN WATFIV REGISTERS
         BR 14    RETURN
A        DC F'16807'
CHAR     DC F'1073741824'
P        DC F'2147483647'
         END
```

BIBLIOGRAPHY

Andersen J.U.,Augustyniak W.M.,Uggerhoj, Phys. Rev. B,3,#3,705(1971)

Anderson C.D., Phys Rev. 43,491 (1933)

Becker E.H. et al, J.of Phys. F1,806 (1971)

Behnisch, Bell, Sizmann, Phys. Stat. Sol. 33,375, (1969)

Berko S.,Plaskett J.S., Phys Rev. 112,1877 (1958)

Berko S., Kingston Positron Conference Proc., p1.175 (1971)

Campbell J.L., Shulte C.W., Mackenzie I.K., Phys.Lett. 38A,#5 (1972)

Carbotte J.P., Arrora H.L., Can. J. of Phys.,45,387 (1967)

Chuang S. Y., Ph.D. thesis, U. of Manitoba (1968)

Davis F. I. , Berko S., Am. Phys. Soc. Bull.,sec 2,8,74 (1963)

Davis J.A., Ericksson L.,Whitton J.L.,Can. J. of Phys.,46,573 (1968)

DeBenedetti S. et al, Phys. Rev.,77,205, (1950)

DeBlonde G., Ph.D. thesis, U. of Manitoba (1972)

Dekhtyar I. Ja.,Mikhalenkov V.S., Sov. Phys. Doklady ,
5,739,(1960);6,31,(1961);6,917 (1962)

Dekhtyar I. Ja., Phys. Lett. 30A,8,462 (1969)

Dekhtyar I. Ja.,Mikhalenkov V.S., Cizek A.,Phys Stat. Sol.(b),
47,K117 (1971)

Dekhtyar I. Ja.,Mikhalenkov V.S., Phys. Stat. Sol.(b),47,K121(1971)

Dirac P.A.M., Proc. Cambridge Phil. Soc.,26,361 (1930)

Ericksson L.,Davies J.A.,Jespersgard P.,Phys. Rev., 161,219 (1967)

Faraci G.,Quercia I.F., Spadoni M.,Turrisi E., Il Nuovo Cimento,
60B,#1, 228 (1969)

Faraci G.,Foti G.,Turrisi I.F., Phys. Lett.,31A,#8,427 (1970)

Faraci G. et al, Phys. Rev. B, 2,7,2335 (1970)

Faraci G., Kingston Positron Conf. Proc., p1.85 (1971)

Ferrell R.A., Rev. Mod. Phys., 28,308 (1956)

Garwin R.L., Phys. Rev.,91,1571 (1953)

Goldanskii V.I., Atomic Energy Rev.,6,#1 (1968)

Gould A.G., Ph.D. thesis, U. of Manitoba (1972)

Heitler W., The Quantum Theory of Radiation, 3rd Ed., Oxford Univ. Press,London and New York

Hyodo T., Sueoka O.,Fujiwara K.,J. of Phys. Soc. of Japan, 31,#2,563 (1971)

Kerr D., Hogg B.G., J. Chem. Phys., 36,2109 (1962)

Kittel C., Introduction to Solid State Physics, 3rd. Ed.

Lee-Whiting, G.E. Phys. Rev. 97,1557 (1955)

Lewis P.A.W. et al, I.B.M. Systems J. ,8,136 (1969)

Lindhard J., Mat.-Fys. Medd. Dan. Vid. Selsk., 34,#14 (1965)

Mohorovicic S., Astron. Nachr., 253,94 (1934)

Ore A., Powell J.L., Phys.Rev.,75,1696 (1949)

Proceedings of the 2nd International Positron Conference, Kingston,Canada (Eds.- A.T. Stewart & B.S. McKee), 1971

Ruark A.E., Phys. Rev. 68,278 (1945)

Senicki E., Ph.D. thesis, U. of Manitoba (1972)

Shearer J.W.,Deutsch M., Phys. Rev., 76,462 (1949)

Siegbahn K.,(Ed.) Alpha-Beta-Gamma Ray Spectroscopy, vol 1 & 2, North Holland Pub. Co. (1966)

Stewart A.T., Roellig L.O., Positron Annihilation, Acad. Press,N.Y. (1967)

Stewart A.T. et al, Phys. Rev., 128,118 (1962)

Stewart A.T., Can. J. of Phys., 35,168 (1957)

Stroud D., Ehrenreich H.,Phys. Rev., 171,399 (1968)

Uggerhøj E., Andersen J.U., Can. J. of Phys., 46,543 (1968)

Vorobev A.A. et al, Phys. Stat. Sol.(a) 6,389 (1971)

Walker R.L. et al, Phys. Rev. Lett.,25,#1,5 (1970)

West R.N., Solid State Comm., 9,1417 (1971)

Yang C.N., Phys. Rev., 77,242 (1950)